Agricultural and Forest Meteorology 306 (2021) 108436

Contents lists available at ScienceDirect

Agricultural and Forest Meteorology

journal homepage: www.elsevier.com/locate/agrformet

Detecting the oak lace bug infestation in oak forests using MODIS and meteorological data

Anikó Kern [a,*], Hrvoje Marjanović [b,*], György Csóka [c], Norbert Móricz [d], Milan Pernek [e], Anikó Hirka [c], Dinka Matošević [e], Márton Paulin [c], Goran Kovač [f]

[a] Department of Geophysics and Space Sciences, Eötvös Loránd University, Pázmány P. st. 1/A, Budapest H-1117, Hungary
[b] Department of Forest Management and Forestry Economics, Croatian Forest Research Institute, Cvjetno naselje 41, Jastrebarsko HR-10450, Croatia
[c] Department of Forest Protection, NARIC Forest Research Institute, Hegyalja str. 18, Mátrafüred H-3232, Hungary
[d] Department of Ecology and Forest Management, NARIC Forest Research Institute, Várkerület 30/A., Sárvár H-9600, Hungary
[e] Department of Forest Protection and Game Management, Croatian Forest Research Institute, Cvjetno naselje 41, Jastrebarsko HR-10450, Croatia
[f] Forest Management Service, Sector for Planning, Analysis, Forest Management and Informatics, Croatian Forests Ltd., Ulica kneza Branimira 1, Zagreb HR-10000, Croatia

ARTICLE INFO

Keywords:
Space-borne remote sensing
MODIS NDVI
Invasive species
Pest detection
Infestation spread
Statistical modelling

ABSTRACT

The oak lace bug (*Corythucha arcuata*, Say 1832) is a new invasive sap-sucking species in the European oak forests that was first recorded in Central Europe in 2013. It invaded the region from Southeastern Europe, spreads rapidly, and shows no signs of receding after establishment. In this study, focusing on the oak forests in the transboundary area of Hungary and Croatia, we applied two novel methods for detecting and assessing the impact of the oak lace bug (OLB) during the period 2000–2019 based on MODIS NDVI measured at 250 m spatial and 8-day temporal resolution. The first detection method is based purely on NDVI and has the potential to be used in near real-time detection. The second one, based on the residual *Z-score* of the NDVI models using daily meteorological and soil water content data as independent variables, aims at improved OLB damage assessment by decoupling the effects of the OLB from those caused by the environmental drivers. The presented detection methods had 61.1% to 93.8% agreement with the *in situ* data, with a better agreement in forests with high oak share. The overall share of the false-positive OLB detections for the strictest method of model residuals was 1.8%. The results confirmed a strong and year-to-year persistent NDVI decrease (down to -14.5% in pure oak forests) during the late summer which can be attributed to the OLB. The origin of the infestation in the study area was identified to be near a resting station on the major highway from Southeastern to Western Europe, corroborating the assumptions that the OLB spread was primarily facilitated by the transport system. The detected speed of the OLB radial spread in the first 3 years of infestation was under 6 km y^{-1}, but since then it increased to above 50 km y^{-1}.

1. Introduction

European forests are expected to play a major role in the EU's climate change mitigation efforts of a 55% reduction in greenhouse gas emission by 2030 and achieving climate-neutrality by 2050 (COM, 2020a, 2020b). However, the climate change itself and the increasing pressure on forest ecosystems imposed by new pests threaten these goals by endangering the longevity, productivity, carbon sequestration capacity, biodiversity, and other ecosystem services of forests (Hlásny and Turčáni, 2008; Wolf et al., 2008; Hicke et al., 2012; Klapwijk et al., 2013; Seidl et al., 2014; Anderegg et al., 2015; Moreau et al., 2020).

The oak lace bug (*Corythucha arcuata*, Say 1832 - Heteroptera: Tingidae), native to North America (Barber, 2010), is a new invasive alien species in Europe, spreading rapidly and causing foliage damage primarily of oak trees, potentially jeopardizing the long term health, productivity and stability of natural oak forests. Since it was first recorded in northern Italy in 2000 (Bernardinelli, 2000; Bernardinelli and Zandigiacomo, 2000), the oak lace bug (hereafter OLB) has spread to most of the countries in South-East and Central Europe (Fig. 1), mostly passively by the traffic and to a lesser extent by the wind (Csóka et al., 2013; Dobreva et al., 2013; Hrašovec et al., 2013; Tomescu et al., 2018; Sotirovski et al., 2019; Mertelík and Liška, 2020). The pest arrived in the

* Corresponding authors.
E-mail addresses: anikoc@nimbus.elte.hu (A. Kern), hrvojem@sumins.hr (H. Marjanović).

https://doi.org/10.1016/j.agrformet.2021.108436
Received 4 January 2021; Received in revised form 23 March 2021; Accepted 8 April 2021
Available online 3 May 2021

region of the Carpathian Basin from the Southeastern direction, where it was first recorded in 2013 in Croatia and Hungary (Csóka et al., 2013; Hrašovec et al., 2013), affecting the valuable pedunculate oak forests of the Pannonian Plain. In recent years the infestation has gained momentum (Simov et al., 2018; Csóka et al., 2020; Paulin et al., 2020), which might be promoted also by the drier weather and delayed arrivals of winter in the region in the last years (Csepelényi et al., 2017a).

All Central European native oaks are suitable hosts for the OLB, but it can occasionally develop on other hosts as well (Csóka et al., 2020). The outbreak populations in Central Europe were most commonly found on pedunculate oak (*Quercus robur* L.), Hungarian oak (*Quercus frainetto* Ten.), sessile oak (*Quercus petraea* (Matt) Liebl.) and Turkey oak (*Quercus cerris* L.) (Csóka et al., 2020). Damage to the leaves caused by the OLB (as a result of leaf-sucking) negatively affects leaf photosynthesis. Nikolić et al. (2019) found a 58.5% decrease in the rate of photosynthesis in the case of pedunculate oak, where the transpiration and stomatal conductance were decreased as well. The OLB, after overwintering in bark crevices and mosses on trees, has 2-3 new generations during the year from April until October/November (Connell and Beacher, 1947). Foliar damage due to the intensive feeding of more generations becomes pronounced in the second part of the vegetation season as early discolouration of the upper surface of the leaves (Bernardinelli and Zandigiacomo, 2000; Paulin et al., 2020). In the case of heavy infestation, premature leaf and acorn abscission could occur, although the negative effects on tree regeneration have not been proven so far (Franjević et al., 2018).

Unlike other disturbances (e.g. the gypsy moth (*Lymantria dispar*); de Beurs and Townsend, 2008; Csóka et al., 2015), the trees cannot recover from the OLB caused damage still in the same growing season. As an alien species in Europe, the OLB has no significant natural predator or disease to control its population (Paulin et al., 2020). So far, only a few naturally occurring native enemies (Paulin et al., 2020) and entomopathogenic fungi (Kovač et al., 2020) have been identified as potential candidates for use in biological control of the OLB population in the region. As a consequence, after establishing itself in a forest stand, the OLB unceasingly affects the oak trees and decreases tree productivity during many consecutive years. The long-lasting effects of such year-by-year reduced photosynthetic capacity due to the OLB are not yet known, however, it likely affects the carbon cycle, and the strong infestations could contribute to increased tree dieback (Dietze and Matthes, 2014). Based on the *in situ* observations, during 2013–2019 there was no other significant pest or disease outbreak in the region affecting the oak forests with similar severity. The role of such *in situ* observations made by entomologists and foresters is indispensable but limited to the relatively low spatial and temporal resolution due to resource constraints (Chen and Meentemeyer, 2016).

Remote sensing provides a valuable tool for monitoring the plant status over large areas with regular spatial resolutions, short repeat time, and in some cases long time-series of data. The detection of forest disturbances by remote sensing has a broad literature (e.g. Fraser et al., 2005; Jin and Sader, 2005; Solberg et al., 2006; Spruce et al., 2011; Griffiths et al., 2014; Meng et al., 2018; Imanyfar et al., 2019), and has also been used in national forest health and early disturbance monitoring systems (Hargrove et al., 2009; Barka et al., 2018; Somogyi et al., 2018). Despite its relatively coarse spatial resolution, many studies have demonstrated the applicability of the high temporal resolution and exceptionally long datasets of the Moderate Resolution Imaging Spectroradiometer (MODIS) for the regional-scale assessment of the insect-caused forest disturbances (de Beurs and Townsend, 2008; Eklundh et al., 2009; Verbesselt et al., 2009; Bright et al., 2013; Olsson et al., 2016a, 2016b).

The Normalized Difference Vegetation Index (NDVI), derived from the measured reflectances in the red and near-infrared parts of the spectra, correlates strongly with the chlorophyll content and the photosynthetic activity of the leaves (Huete et al., 2002). Therefore, it is one of the most commonly used remote sensing vegetation index (VI) in detecting the infestation and studying the pest impact on the forest canopy (e.g. Spruce et al., 2011; Hargrove et al., 2009; Spruce et al., 2019). The pest damage is often quantified also with other spectral indices (de Beurs and Townsend, 2008; Eklundh et al., 2009; Verbesselt et al., 2009; Townsend et al., 2012; Sangüesa-Barreda et al., 2014), or by the reduction of some derived parameters like the Gross Primary Productivity (GPP), Net Primary Production (NPP), or Leaf Area Index (LAI) (e.g. Bright et al., 2013; Olsson et al., 2017).

Most of the existing studies on pest detection or pest disturbance assessment were based either on the yearly maximum VI (e.g. de Beurs and Townsend, 2008; Spruce et al., 2011) or the VI anomaly, i.e. the difference between the VI in the year when the pest was present and the

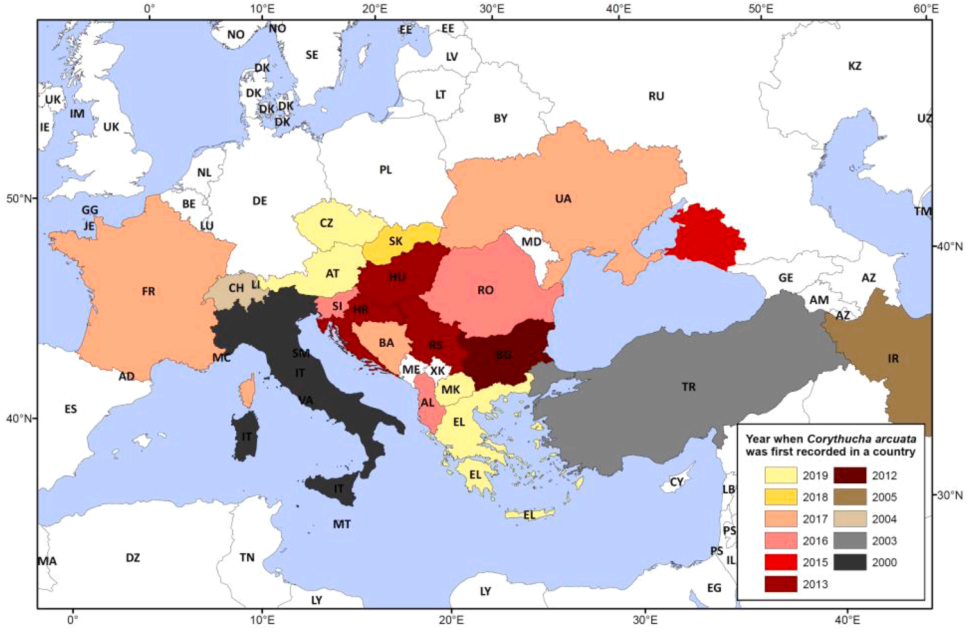

Fig. 1. Map of the spread of the oak lace bug in Europe and the Middle East. The map shows the years of the first records in the countries. (Source of data: https://gd.eppo.int/taxon/CRTHAR/distribution, Sotirovski et al. (2019) for North Macedonia, and Mertelík and Liška (2020) for Czechia).

VI mean of the years preceding the pest disturbance serving as the reference (Eklundh et al., 2009; Townsend et al., 2012; Griffiths et al., 2014; Olsson et al., 2016b; Spruce et al., 2019). In such studies, the effects of the yearly meteorological and soil moisture conditions on the plant phenology are rarely taken into account explicitly. Recognizing the importance of the interannual variability of the phenology in the calculation of the pest-related VI anomaly, Chávez et al. (2019) proposed a method to reconstruct the annual phenology based on the frequency of the VI density, expressing the probability of the observed anomaly. Accounting for the effects of the weather and soil moisture on the interannual variability of VI is important in the pest damage assessment and modelling, particularly in the case of long-lasting infestations. Decoupling of those effects in VI modelling so far has been rare and still presents a challenge.

The objective of the present study was to (i) identify forest areas with a high probability of OLB infestation by creating novel detection methods based on 20-year long MODIS NDVI data with 250 m spatial resolution for the transboundary area of Hungary and Croatia; (ii) create and validate NDVI models that will facilitate decoupling of the effects on the NDVI caused by the OLB from the effects caused by the year-to-year variability in weather, changing soil water content and forest management; (iii) assess and quantify the decrease in forest NDVI in the selected period of the growing season with respect to the different forest categories and the share of oaks in a pixel; and (iv) map the OLB spread in the study area and estimate its speed based on the detected infested pixels.

2. Materials and methods

2.1. Study area

The target area of this study was the most OLB-infested parts of Croatia and Hungary, namely the Northeastern part of Croatia and the Southwestern part of Hungary, located in Central Europe (Fig. 2), between 44.84–46.8°N and 16.4–19.45°E. The Hungarian part of the study area was selected as the area in Hungary which showed the highest infestation level in 2019 based on the *in situ* field observations (see below, Section 2.2). The Croatian part was selected to involve the starting location of the spread in Croatia, in the Spačva forest (Hrašovec et al., 2013). Spačva forest, as part of the Slavonian oak forests, is the largest pedunculate oak forest complex in Europe (Klepac and Fabijanić, 1996) and served as an ideal breeding ground for the OLB showing high infestation intensity since 2016 (this study). According to the Köppen-Geiger classification scheme the climate of the area is warm temperate, with no dry season and warm to hot summers, corresponding to climate classes Cfb (in the West) and Cfa (in the East), respectively (Rubel and Kotek, 2010).

2.2. Presence of the OLB in the study area based on field observations

In the Hungarian part of the study area, the OLB was first recorded in 2016 and the first larger infestation was reported in 2017 (Csepelényi et al., 2017b). In the Croatian part, the OLB was first found in Spačva forest, where the spread started in 2013. Therefore, relying on the *in situ* observations of the study areas, the *pre-"oak lace bug era"* (hereafter *PreOLB-era*) of the applied MODIS dataset can be considered as 2000–2016 and 2000–2012, and the *oak lace bug era* (hereafter *OLB-era*) as starting from 2017 and 2013, in the case of Hungary and Croatia, respectively. The Hungarian *in situ* observations of the OLB in the forest compartments are recorded in the *Hungarian National Forest Damage Registration System* (NFK, 2020) regularly since 2019 and in the case of Croatia within the national system for *Reporting and Forecasting in Forestry* – IPP (Matošević, 2020) since 2016. The OLB monitoring in Croatia is conducted at the level of forest management unit (FMU, average area ~3 kha) on 68% of the forests (193 FMUs) in the Croatian part of the study area.

The records on the *in situ* presence of the OLB in the monitored forest compartments (Hungary) and FMUs (Croatia) were used to test the agreement with the detection results based on the methods presented in this work.

2.3. Remote sensing based dataset

To quantify the impact caused by the OLB in terms of remote sensing, official products created from the data of the MODIS sensor on-board satellite Terra were used with the finest available spatial resolution (Justice et al., 1998). We calculated NDVI from the Collection 6 MOD09Q1 surface reflectance product with 250 m spatial and 8-day temporal resolution (Vermote, 2015) for the study period of 2000–2019. The temporal composite MOD09Q1 contains atmospherically corrected surface reflectances for the visible bands in 8-day periods, resulting in 46 data per year for each pixel. To create NDVI the

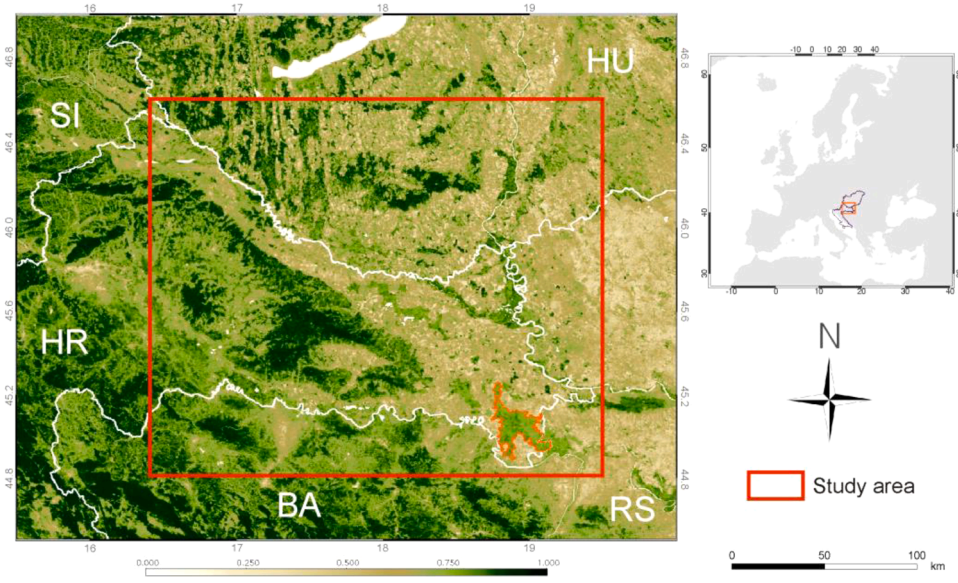

Fig. 2. Map of the Hungarian and Croatian study areas located in Central Europe (the base of the map is a MODIS NDVI image from the beginning of September 2019). The Spačva forest in SE Croatia, where the OLB was first detected in the study area in 2013, is delineated with a red line.

surface reflectances of Band-1 (ρ_{RED}, in visible red) and Band-2 (ρ_{NIR}, in near-infrared) of the sensor were used, where NDVI is defined as $(\rho_{NIR} - \rho_{RED})/(\rho_{NIR} + \rho_{RED})$. The Hierarchical Data Format (HDF) files of the MOD09Q1 product contain Julian date information and State and Quality Control (QC) flags as well at the pixel-level, where the time-stamp of the data refers to the exact dates when they were measured. Data for the tile h19v04 were downloaded from NASA LP DAAC (LP DAAC, 2020).

Processing all of the datasets of the present study and execution of the calculations were performed using the Interactive Data Language (IDL) version 8.6 (Harris Geospatial Solutions, USA), and STATA 14.2 (StataCorp., USA).

The flowchart of the applied methodologies presented in the following sections is shown in Fig. S1 in the Supplementary Material.

2.3.1. Creating smoothed NDVI time-series from the raw MODIS reflectance dataset

The first step in obtaining a quality filtered and smoothed NDVI time-series at a regular grid with 8-day temporal resolution was the pre-processing of the raw dataset containing information on the exact Julian dates of the reflectance measurements, based on the work of Kern et al., 2016 and 2020, where only data with the strictest quality criteria were kept. To avoid any misleading and non-realistic sudden NDVI decrease due to the presence of unrecognized and incorrectly quality flagged atmospheric effects (such as high aerosol content, presence of thin cirrus, sub-pixel clouds, etc.), the Best Index Slope Extraction (BISE) method (Viovy et al., 1992) was applied at the pixel-level. The quality checked and gap-filled NDVI dataset was then resampled into daily resolution using linear interpolation, where the actual Julian dates of the measurements were taken into account. Then, the widely used Savitzky-Golay filter (e.g., Chen et al., 2004; Eklundh et al., 2009; Spruce et al., 2011) was applied with a moving time window of 15 days to smooth the dataset using the built-in IDL SAVGOL and CONVOL routines. From the smoothed daily resolution dataset only 46 data points were preserved for each year, corresponding to the middle of the original 8-day periods. This smoothed NDVI dataset at a regular 8-day resolution time step served as the basis for our investigations.

2.4. Meteorological and soil water content dataset

To investigate the effects of the weather and other environmental conditions on the vegetation during the late summer meteorological data of the FORESEE database (Dobor et al., 2014) and soil water content of the ERA5-Land dataset (Balsamo et al., 2009) were used. FORESEE contains observed and projected daily maximum/minimum temperature [°C] and precipitation fields [mm day^{-1}] for the wide region of the Carpathian Basin (42°35'–51°05'N, 10°55'–28°05'E) on a regular grid with a spatial resolution of 1/6° × 1/6°, covering the 1951–2100 period. Daylight average shortwave radiative flux (in other words global radiation; [W m^{-2}]) was calculated on the same grid using the MTClim model (Thornton et al., 2000), and multiplied with the corresponding day length (in seconds) to get the values in MJ m^{-2} day^{-1}. The three-hourly ERA5 Land volumetric soil water [m^3 m^{-3}] were downloaded from the Copernicus site (CCCS, 2019) with 0.1° × 0.1° spatial resolution for two different soil layers (3rd and 4th layer at 0.28–1 m and 1–2.89 m depth, respectively) of the study area, and were used to create daily mean soil water content (SWC) values during 2000–2019.

The daily data stored at the original grid of FORESEE and ERA5 were resampled to the finer grid of the MODIS products using linear interpolation. In the case of temperature and precipitation, the resampling was performed based on the methodology of Kern et al. (2016), where the elevation of the pixels was also taken into account.

2.5. Land cover datasets with spatially explicit tree species distribution information

2.5.1. Land cover datasets

Since the study area is part of two countries, two different national land cover datasets were utilized. For Hungary, the *National Ecosystem Base Map* land cover dataset of the NÖSZTÉP project (Tanács et al., 2019; http://web.map.fomi.hu/nosztep_open/) was used to distinguish the land cover types with the available species information. This newly published land cover dataset (hereafter referred to as NÖSZTÉP) has 56 different categories at Level-3 with a 20 m spatial resolution, stored in Lambert Azimuthal Equal Area projection, covering entire Hungary. In the present study, this Level-3 dataset was at first reprojected to WGS-84, and then overlapped with the 250 m resolution (QKM) MODIS grid. This enabled the calculation of the share of each of the 56 NÖSZTÉP Level-3 categories within every MODIS pixel. Table S1 in the Supplementary Material lists the Level-3 categories of the NÖSZTÉP's *Forest and Woodlands* (Level-1) category, as well as the number of the QKM pixels with respect to the predefined minimum share of a given Level-3 category within the pixels. The base year of the thematic dataset was 2015, which was partially improved by high-resolution remote sensing data (Sentinel-1 and -2) from the year 2017 (Tanács et al., 2019). The land cover map of the Hungarian study area at the QKM grid with the dominant NÖSZTÉP category of each pixel is shown in Fig. S2a, while the corresponding legend is presented in Fig. S2b in the Supplementary Material.

In the case of Croatia, the main source of the land cover data was the database *HŠ Fond* of the Croatian Forests Ltd. The *HŠ Fond* is the national forestry database containing data from both state and private forests including spatial information on forest area division down to forest sub-compartments as elementary units. Basic data on forests from the *HŠ Fond* database are also available to the public (http://javni-podaci.hrsume.hr/). The following data from the *HŠ Fond* database were used for all forest sub-compartments (excluding those containing stands younger than 20 years or those categorized as shrubs): volume of standing live trees, estimated annual increment, year of harvesting/thinning/salvage logging, and volume of cut trees, all according to the different tree species. The living tree volume and increment are measured once every ten years in preparation of the forest management plans. Using the above data, we modelled the volume of the living trees (at species level) by adding the estimated increment to the initial volume and subtracting the harvest recorded in that year. The result was for every forest sub-compartment, the sequence of annual values for the living trees volume, increment and harvest at the species level (expressed in m^3 ha^{-1}) for all years of the study period, namely 2000–2019.

In the next step, the forest sub-compartment polygons were intersected with the MODIS QKM pixel grid projected in the local HR_ETRS89/TM geographic reference system (EPSG: 3765) using QGIS 3.10.2 with GRASS7.8.2 GIS software (an example shown in Fig. S3 in the Supplementary Material). Finally, the forested area, the volume, the increment, and the harvest (all by tree species) were calculated for every MODIS QKM pixel in every year during the period 2000–2019.

2.5.2. Pixel selection

Pixel selection criteria for the Hungarian and Croatian parts of the study area was mostly uniform, but also included some additional country-(i.e. dataset)-specific criteria. The uniform part of the pixel selection procedure consisted of two steps. In the first step pixels not reaching the minimum of 95% forest cover were discarded. This step was applied to secure that the signal from the non-forest areas (in particular due to croplands and grasslands) remains low. In the second step, the forest share of the side-neighbouring pixels to those that passed Step 1 was checked, and those which did not reach the minimum forest cover of 60% were also excluded. This filtering criterion was applied due to the known geolocation inaccuracy of the MODIS measurements

(Wolfe et al., 2002) and due to the artefacts of the gridding procedure (Tan et al., 2006) and possible re-projection inaccuracies. The used 60% threshold was chosen based on a preliminary assessment of the potential impact of the above-mentioned confounding effects and the need to retain as many pixels as possible.

For the Hungarian part of the study area, an additional filtering step was designed due to the lack of forest management data. The possible forest management events (e.g. stand harvesting) or possible massive abiotic disturbances that could have occurred (e.g. windthrow) in a pixel were detected based on the mean NDVI of the main part of the growing season ($NDVI_{19\_31}$; 19th to 31st MODIS 8-day period, corresponding to 25 May – 5 Sep). The starting and the ending 8-day period of the main part of the growing season were determined to reflect a general period when the phenology of all forest pixels in the study area (and during all years of the study period) has surely passed the End of Green-up (EoG) in spring but has not reached the Onset of Senescence (OoS) in autumn. The latest EoG and the earliest OoS were calculated using the 20% cut-off method (Hargrove et al., 2009; Shen et al., 2015; Wang et al., 2018; Kern et al., 2020). The threshold of the $NDVI_{19\_31}$ was set to 0.8 based on the distribution of the $NDVI_{19\_31}$ values during the *PreOLB-era*. Pixels below the threshold in any of the years during the investigated 2000–2019 period were excluded from the dataset.

For the Croatian part data on standing tree volume and annual harvests at the species level were available for every pixel during the period 2005–2019. Consequently, the effects of forest management were addressed by excluding all pixels having total harvesting intensity in the period 2005–2019 above 35% or those containing less than 50 m^3 ha^{-1}.

2.5.3. Categorization of the selected pixels according to dominant tree species

Tree pests and diseases frequently occur exclusively or, as is the case with the OLB, have a preference for particular tree species. The observed damage from the pest is generally proportional to the share of the targeted tree species and the density of the pest (severity of the "attack"). Therefore, the share of the oaks (*Quercus* sp.) and other accompanying tree species had to be considered in every pixel.

Table 1 lists the created forest groups indicating the number of pixels within each group for each country. For Hungary, the pixel categorization was based on the share of areas of NÖSZTÉP Level-3 categories.

Table 1
The number of the selected MODIS QKM pixels according to the defined forest groups.

Investigated species groups	n - Hungary	n - Croatia
Pure groups		
Pure pedunculate oak (*Q. robur*)	N/A	390
Pedunculate oak with narrow-leaved ash (*Q. robur* & *F. angustifolia*)	150	1467
Pedunculate oak with common hornbeam (*Q. robur* & *C. betulus*)	136	1606
Sessile oak with common hornbeam (*Q. petrea* & *C. betulus*)	491	131
Turkey oak (*Q. cerris*)	476	31
Pubescent oak (*Q. pubescens*)	23	4
Sessile oak with common beech (*Q. petrea* & *F. sylvatica*)	N/A	1215
Pure ash (*F. angustifolia*)	N/A	114
Pedunculate oak (mixed) [a]	442	N/A
All oaks [b]	2048	N/A
Extended groups		
Oaks above 50% share (*Quercus* share >50%)	5,217	8,711
Oaks above 20% share (*Quercus* share >20%)	7485	17,013
Additional groups		
Oaks below 10% share	5775	5013
Leftover forested	18,146	18,322

[N/A] Due to differences between the Hungarian and Croatian forest datasets the group is not applicable for this country.
[a] All NÖSZTÉP Level-3 categories with pedunculate oak in a pixel combined.
[b] All NÖSZTÉP Level-3 categories with any kind of oak in a pixel combined.

Pixels having at least 95% of the area covered by the corresponding forest type were selected for this study. Categorization with respect to forest groups in the case of Croatia was based on the volume shares of different tree species. Pure oak groups contained pixels with >85% share of corresponding oak species in the total volume of live trees in a pixel. Pure groups of *oak with other species* (common hornbeam or narrow-leaved ash) contained 50–85% of oak and the *other species* was by its volume share second after oak. Fig. 3 shows the map of the selected pixels by the defined forest groups.

Pure groups contain pixels in which only one forest type is predominantly (>95%) present (Hungary), or the volume share of the dominant tree species in a given forest group is greater than 50% (Croatia). It is important to keep in mind that, due to the high degree of land cover diversity and the coarse MODIS resolution (250 m), by using only *Pure groups* we would discard a lot of forested pixels containing more forest types. To avoid this, we created and tested two extended groups: the *Oaks above 50% share* and the *Oaks above 20% share*. Pixels dominated by pubescent oak (with 95% share), and in the case of Croatia also by Turkey oak were dropped from the study due to the low pixel numbers. The additional group *Oaks below 10% share* contained pixels having less than 10% oaks and ashes (*Fraxinus* sp.) and served as a control group. The reason behind excluding narrow-leaved ash was the emergence of the ash dieback fungus (*Hymenoscyphus fraxineus*, previously known as *Chalara fraxinea*) in Central Europe, the first time recorded in Hungary in 2008 (Szabó, 2008) and in Croatia in 2011 (Barić et al., 2012; Matošević, 2012).

Finally, the *Leftover forest* group contained forested pixels which did not meet the selection criteria and served only for the visualization of the forested area.

2.6. Identification of pixels with OLB-like damage based only on the remote sensing data (RS method)

The identification of the pixels with typical OLB-like damage was based on the observable NDVI decrease in a pre-defined period (see below) due to damage from the feeding activity of the OLB. This becomes observable by remote sensing as the decrease in the NDVI already in late July. The NDVI decrease becomes strong from the second part of August when the possible second generation of the OLB emerges (Franjević et al., 2018). Table 2 presents the exact dates of the MODIS 8-day periods during the year relevant from the remote sensing perspective to the monitoring of the OLB damage.

Considering the above, the strongest NDVI decrease (observed as the sharpest NDVI decrease due to the OLB) happens during the late summer and the beginning of autumn (~30th to 33rd MODIS 8-day period during the year). The decrease in the NDVI continues afterwards as well, but it is difficult to attribute it solely to the OLB. The earliest recorded onset of senescence in the study area in the *PreOLB-era* was the 33rd 8-day period (starting from ~ 14st Sept). To avoid the possible effects of early senescence, the identification of the OLB presence was based on the decrease in the average NDVI during the 30th to 32nd 8-day period (21st of Aug – 13th of Sept, hereafter $period_{30\_32}$). The application of averaging the three consecutive 8-day periods was chosen also to minimize the false identification of pixels as a consequence of any remaining, unidentified noise in the NDVI dataset due to clouds, atmospheric or angular effects.

The RS method for identifying disturbances that could be related to the OLB consisted of two conditions. The basic assumption was that the observed NDVI of a given (*i,j*) pixel shows negative NDVI anomaly during the investigated $period_{30\_32}$ of the given year in the forms of:

$$NDVI_{i,j,p,y} < MeanNDVI_{i,j,p,PreOLB} \text{for } p = 30 - 32, \quad (1)$$

where $MeanNDVI_{i,j,p,PreOLB}$ is the multiannual mean NDVI for the indicated periods during the *PreOLB-era*, and $NDVI_{i,j,p,y}$ are the mean values of the processed NDVI dataset at the pixel-level in the indicated 8-day

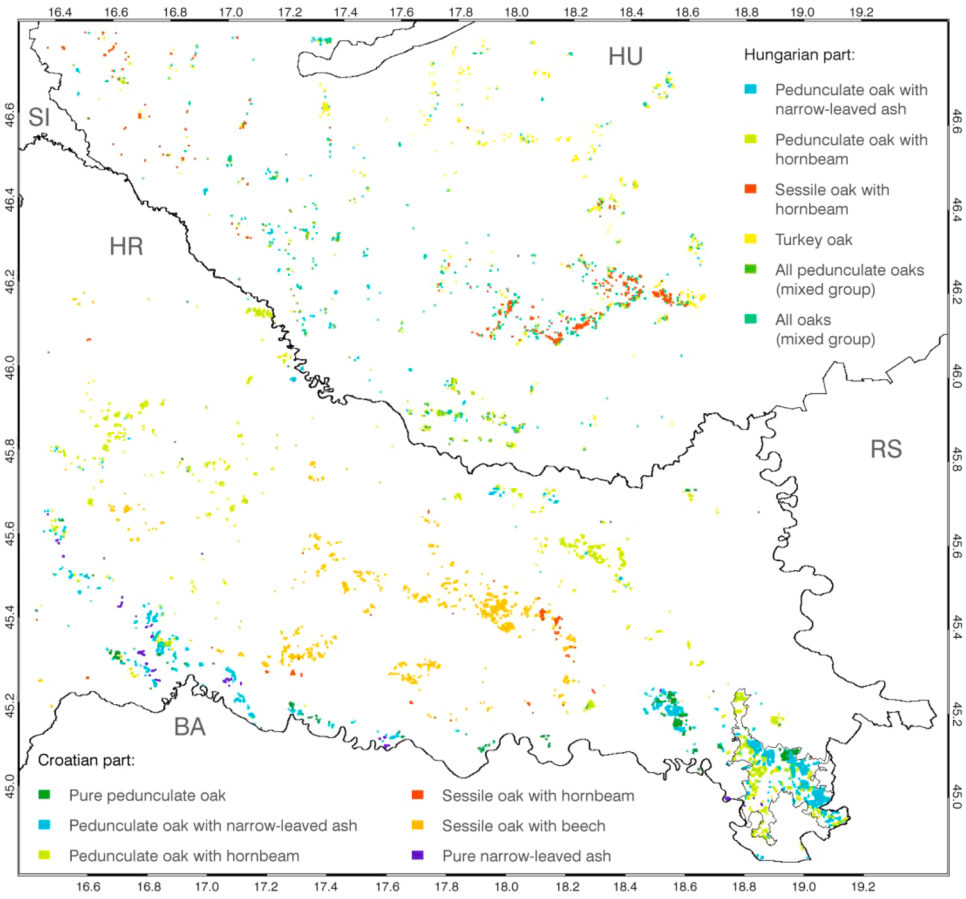

Fig. 3. Map of the used QKM pixels after the strict filtering procedure in the different *Pure* species categories in the study area. (Pixels of the *Extended* and *Additional* groups are not shown)

Table 2
The ordinal number of the MODIS 8-day periods during the OLB affected period of the year, corresponding Julian days of the year (DOY), dates, and comment relevant to the OLB detection.

Number of the 8-day period	Julian days	Date	Description/Comments
25th	193 – 200	12–19th of July	Possible appearance of the second OLB generation
26th	201 – 208	20–27th of July	
27th	209 – 216	28th of July – 4th of August	The OLB caused NDVI decrease might become noticeable
28th	217 – 224	5–12th of August	
29th	225 – 232	13–20th of August	
30th	233 – 240	21–28th of August	Investigated period: used in identification and modelling
31st	241 – 248	28th of Aug. – 5th of Sept.	Investigated period: used in identification and modelling
32nd	249 – 256	6–13th of September	Investigated period: used in identification and modelling
33rd	257 – 264	14–21st of September	The earliest recorded OoS during the PreOLB-era
34th	265 – 272	22–29th of September	Average time for the OoS during the PreOLB-era

periods (p) of the investigated year (y), respectively. The second criterion was based on the mean difference during the *PreOLB-era* between the yearly $MaxNDVI_{i,j,19–29,y}$ and $MinNDVI_{i,j,30–32,y}$ values (where the latter is the yearly minimum NDVI value of the $period_{30–32}$), indicated as $MeanNDVIdiff_{i,j,PreOLB}$. This criterion is defined as:

$$NDVI_{i,j,p,y} < MaxNDVI_{i,j,19-29,y} - MeanNDVIdiff_{i,j,PreOLB} \text{for} \, p = 30 - 32, \quad (2)$$

where:

$$MeanNDVIdiff_{i,j,PreOLB} = \text{mean}\left(MaxNDVI_{i,j,19-29,y} - MinNDVI_{i,j,30-32,y}\right). \quad (3)$$

In the case when both criteria are met, the pixel is classified as damaged for the year in question, likely by the OLB. We assigned a continuity flag (hereafter C-flag) to each pixel containing information about the continuity of the disturbance detection in the subsequent years of the *OLB-era*. Namely, C-flags are: 1 – not detected during the OLB era; 2 – damage detected intermittently in some years; 3 – detected continuously every year since the first year of detection.

2.7. Identification of pixels with OLB-like damage using NDVI model residuals (MR method)

The assessment of the OLB infestation required decoupling the OLB effect on the NDVI from the effects of the main meteorological and environmental variables as well as the effects of other pests and management. To do this, prognostic multiple linear models for the yearly mean NDVI during the investigated $period_{30–32}$ (hereafter $NDVI_{30–32}$) were constructed (Section 2.7.1). The model residuals were used to identify forested pixels which can be linked to the damage from the OLB infestation (Section 2.7.2).

The *MR* method for the OLB detection is based on the assumption that the distribution of the residuals of the NDVI model does not change with time if the independent variables remain within their usual (e.g. calibration) range. If there is a sudden change in the distribution of the

model residuals, i.e. if the model performance suddenly becomes considerably worse while the independent variables are within the usual range, then this is an indicator that some new agent (OLB) additionally affecting the NDVI has appeared.

Using only data from the *PreOLB-era* to avoid the influence of the OLB, the constructed models were calibrated and then validated by applying the leave-out-one-year (LOOY) cross-validation technique (Santos et al., 2011). In the LOOY validation, the model is calibrated with a dataset from which one calendar-year of the data are year-by-year omitted. Model predictions were then tested against the observations in the year that was left out, which was repeated for all years of the validation dataset. When used for prediction, data of the entire *PreOLB-era* were used for model calibration and the model was then applied for the whole study period (2000–2019).

The studied parts of Hungary and Croatia belong to two different biogeographic regions (the Pannonian and the Continental, respectively), where the border between the two biogeographical regions corresponds to the county borders. To reflect the differences due to the geography and the weather, but also due to the land cover datasets and forest management practices, country-specific $NDVI_{30–32}$ models were constructed.

2.7.1. Building of the $NDVI_{30–32}$ model

The NDVI models were build using two kinds of predictor variables at the pixel-level: i) meteorological and environmental variables: daily minimum and maximum temperature (*Tmin* and *Tmax*); the amount of available shortwave solar energy (*Rad*); precipitation (*Prec*); and soil water content at two layers (*SWC3* and *SWC4*); and ii) mean NDVI of periods 25–26 (i.e. before the assumed start of the observable NDVI decrease; hereafter $NDVI_{25–26}$). In the case of the meteorological and environmental variables, the mean (and in the case of precipitation the total) of the 16 days were used. The $NDVI_{25–26}$ served as a proxy variable for non-OLB pest damage and forest management activities, as most of the non-OLB pest activity (e.g. defoliation of oaks by *Lymantria dispar*, or the effects of infestation with the powdery mildew) or management activities (e.g. thinning) reflect on the $NDVI_{25–26}$.

The general theoretical form of the considered $NDVI_{30–32}$ model based on the different averaging periods (AP) of the applied variables was:

$$NDVI_{30-32} = \sum_{AP}(\alpha_{AP}\cdot Tmax_{AP} + \beta_{AP}\cdot Tmin_{AP} + \gamma_{AP}\cdot Prec_{AP} + \delta_{AP}\cdot Rad_{AP} + \varepsilon_{AP}\cdot SWC3_{AP} + \zeta_{AP}\cdot SWC4_{AP}) + \eta\cdot NDVI_{25-26} + constant, \quad (4)$$

where $Tmax_{AP}$, $Tmin_{AP}$, $Prec_{AP}$, Rad_{AP}, $SWC3_{AP}$, $SWC4_{AP}$ are the pixel-level mean of the maximum and minimum temperature, precipitation, radiation, and soil water content at two different layers for a given AP, respectively, and α_{AP}, β_{AP}, γ_{AP}, δ_{AP}, ε_{AP}, ζ_{AP}, and η are model coefficients. The general model (Eq. (4)) has a very large number of predictor variables and would suffer from issues such as co-linearity, overfitting, and lack of interpretability, thus the number of variables in the model had to be reduced. The reduction of the general model by identification of the smallest set of most important variables and time periods was based on the *Lasso* approach, separately for each country.

The Least Absolute Shrinkage and Selection Operator (*Lasso*) was used for selecting the optimal set of predictor variables. The *Lasso* is a regularized regression method which applies λ^1 norm penalization to achieve sparse solutions (Tibshirani, 1996). This technique is suitable for high-dimensional cases where the number of independent variables is large (Ahrens et al., 2020). The selection of the best set of predictor variables was made using STATA 14.2 and the program *cvlasso*, which is part of the package *lassopack* (Ahrens et al., 2020). The applied *cvlasso* uses *k-fold* cross-validation (in our case, each fold was defined by the calendar year) for selecting the penalty level parameter lambda, which optimizes out-of-sample prediction performance by minimizing the mean-squared prediction error. Bayesian Information Criterion (*BIC*), root mean square error (*RMSE*), mean absolute error (*MAE*), bias, and coefficient of determination (Pearson R^2) were used for the assessment of the goodness of the model.

In the next step, the set of independent variables obtained with *cvlasso* was used to perform the model calibration and validation with the ordinary least square regression (OLS). The initial set of predictor variables was further reduced by applying a procedure that is similar to the backward stepwise regression. At first, the model obtained with *cvlasso* was calibrated using the entire *PreOLB* data and all non-significant ($p < 0.05$) variables (if any) were removed one-by-one until only those significant remained. Then, the model was validated using the LOOY cross-validation technique (Santos et al., 2011) based on the *PreOLB* part of the dataset. If some of the variables became non-significant ($p < 0.05$) at any step of the validation, that variable was removed (starting with the least significant one) and the procedure was repeated until all variables were significant at all times. The removal of the least significant predictor variables continued, even if all variables were significant ($p < 0.05$), up to the point when the model with the smallest (or most negative) cross-validation *BIC, RMSE, MAE*, bias and the highest cross-validation R^2 were identified. This extension of the *Lasso* procedure enabled us to find an optimal model with the smallest number of independent (and highly significant) variables and best model performance on the validation dataset. The final models were then calibrated using the *PreOLB* part of the dataset (2000–2016 for Hungary and 2000–2012 for Croatia) and used for the calculation of the *Z-score* (see next section). The model coefficients and the performance statistics were calculated independently using the *IMSL_multiregress* function in IDL and regress function in STATA to assure reliable and error-free results.

2.7.2. Identification of the OLB infested pixels based on the $NDVI_{30–32}$ model residual Z-score

The *Z-score*, or standard score of a data point, is the distance of the data point from the population (sample) mean, expressed in units of standard deviations. Assuming the model residuals are normally distributed, the residual *Z-score* can be used in outlier detection since the *Z-scores* of less than -3 or greater than 3 are typically considered outliers (Misra et al., 2020). For a model that is not biased and which has normally distributed residuals, the share of residuals with $z < -3.09$ would be 0.001, or 0.1%. According to this, the z = -3.09 of the model residuals during the *OLB-era* was used as a threshold for the detection of outlier pixels with unexpectedly negative residual. The unusually low observed NDVI, much lower than expected (modelled) after accounting for the variability caused by the meteorology, soil water content and $NDVI_{25–26}$, served as an indicator of the damage that could be associated with the presence of the OLB. Therefore, all pixels with a residual *Z-score* less than -3.09 were identified as affected by the OLB. The effects of other pests, management activity, or natural disturbance were in most cases already visible on the $NDVI_{25–26}$ and therefore have been accounted for in the model. This emphasizes the essential role of the $NDVI_{25–26}$ in the $NDVI_{30–32}$ modelling. The remaining, unaccounted negative residuals may be (with high probability) attributed to the OLB.

The values of the model residuals during the *PreOLB-era* (i.e., the years 2000–2012 for Croatia or 2000–2016 for Hungary) were used for

the calculation of the mean and the standard deviation of the model residuals at the pixel-level. The *Z-score* of the model residual for an (*i,j*) pixel and *y* year was calculated as:

$$z_{i,j,y} = \frac{\left(r_{i,j,y} - \overline{r}_{i,j,PreOLB}\right)}{s_{i,j,PreOLB}}, \quad (5)$$

where $\overline{r}_{i,j,PreOLB}$ and $s_{i,j,PrePLB}$ is the mean and standard deviation of the model residuals during the *PreOLB-era* for the pixel (*i,j*).

Considering that the number of data points (years) per pixel is small, it could be expected that the assumption of the normality of the residuals' distribution at the pixel-level would not be always met. However, given that the number of the pixels is large, the violation of the normality assumption at the pixel-level may be acceptable (e.g. Zeller and Levine, 1974), especially if the overall distribution of the residuals during the *PreOLB-era* is close to normal distribution. Provided that the residuals are normally distributed and given that the share of pixels with $z < -3.09$ under the normal curve is 0.1%, the probability of error (false-positive) in our case would be 0.1%. If the share of the pixels identified as outliers during the *PreOLB-era* was sufficiently close to the theoretical value of 0.1% we may assume, in line with Zeller and Levine (1974), that possible deviations of residuals from normal distribution did not affect significantly the results.

Assessment of the goodness of the used *Z-score* threshold value regarding the false-negative detections could not be as direct as in the case of false-positive. Therefore we investigated the evolution of the *Z-score* of the infested pixels' residuals from the year when a pixel has been detected as infested by the *MR* method for the first time during the *OLB-era*. The year of the first detection was marked as year zero, and only pixels with C-flag 3 were considered. If the selected threshold (-3.09) is adequate, the average *Z-score* in the year preceding the first year of detection (i.e. in the year = -1) should not be significantly different from zero.

2.8. Assessment of the OLB-caused NDVI decrease

For a given year *y* in the *OLB-era* the model bias ($bias_y$) is the result of two causes: bias due to inherent model limitations ($bias_{0,y}$) and the additional bias ($bias_{OLB,y}$) that is caused by the OLB related decrease in NDVI:

$$bias_y = bias_{0,y} + bias_{OLB,y}. \quad (6)$$

It should be noted that the above equation is a simplification as it does not take into account the possible effects of the meteorology on the OLB activity/abundance. For the years of the *PreOLB-era* the $bias_{OLB,y}$ is zero (by definition), therefore Eq. (6) becomes:

$$bias_y = bias_{0,y} = \frac{1}{n}\sum\left(NDVI_{modelled,30-32,y} - NDVI_{observed,30-32,\ y}\right), y \in PreOLB - era \quad (7)$$

where *n* is the number of pixels.

The average decrease of the $NDVI_{30-32}$ of the detected pixels that is caused by the OLB in a given year corresponds to the mean residual of the infested pixels, corrected for the inherent model bias for that year ($bias_{0,y}$). The model $bias_{0,y}$ could not be calculated for the years in the *OLB-era*, therefore it was approximated with the average of the model biases during the *PreOLB-era* (Eq. (7)), obtained by the LOOY cross-validation. The average decrease in $NDVI_{30-32}$ ($\overline{D}_{30-32,\ y}$) of the OLB infested pixels in a given year *y* is calculated as:

$$\overline{D}_{30-32,\ y} = \overline{residual}_{infested,\ y} - bias_{0,y} \approx \overline{residual}_{infested,\ y} - \overline{bias}_{preOLB}, \quad (8)$$

where $\overline{residual}_{infested,\ y}$ is the mean model residual of the infested pixels in year y, $\overline{residual}_{infested,\ y}$ is the cross-validation mean bias during the *Pre-OLB-era*. The standard error ($se_{D,y}$) of the $\overline{D}_{30-32}$ in a year *y* is:

$$se_{D,y} = \sqrt{se^2_{residual\ \ infested,y} + se^2_{bias,\ PreOLB}} \quad (9)$$

where $se_{residual\ \ infested,y}$ is the standard error of the mean residual of the infested pixels in a given year *y* and $se_{bias,\ PreOLB}$ is the standard error of the mean bias during the *PreOLB-era*, obtained with cross-validation.

2.9. Comparison of the RS and MR detection and agreement with the in situ records

The agreement of the results of the *RS* and *MR* detection methods were compared with McNemar's test for the equality of the marginal frequencies (McNemar, 1947). For pixels detected as infested, a status of the detection in the following year was examined to check the agreement between the methods and the continuity of the detection.

The validation of the methods in the strictest sense, where each MODIS pixel area corresponding to the same validation area would be monitored every year and the presence or the absence of the OLB would be recorded, was not possible because such data do not exist. Therefore, the existing albeit very short (Hungary) or coarse (Croatia) records of the *in situ* OLB presence were used for the comparison with the detection results of the *RS* and *MR* methods. The McNemar's test was again used for testing the differences between the *RS* and *MR* detection methods against the records of the *in situ* OLB presence.

2.10. Locating the origin of the infestation and calculating the rate of the OLB spread

Using the *RS* and *MR* methods for identification of the infested pixels we created maps showing the detected spread of the OLB infestations based on the year of the first detection. Also, both the *RS* and *MR* methods were used to reconstruct the origin of the OLB spread in the study area and to test the agreement with the field observations. The origin of the OLB spread was determined as the centroid (geographical mean) of the infested pixels detected in 2013 (as the first year) in the area of Spačva forest. The maps and calculations were made with QGIS 3.10.2 with GRASS 7.8.2 and ESRI ArcGIS 10.1 Desktop software.

By setting the origin of the infestation as the centre of the coordinate system, the mean radial distance of the newly infested area (pixels) was calculated for every year using only continuously detected pixels (with C-flag 3). The mean annual radial speed of the spread (in km y^{-1}) for a given year was calculated as the difference between two consecutive mean radial distances divided by one year.

3. Results

3.1. Detecting pixels with OLB-like damage based on the RS method

Using the *RS* method we discriminated the possible infested pixels from the probably not infested ones. However, it is important to note that at this point we still cannot claim that the detected NDVI decrease of a pixel is only attributed to the OLB or if other biotic or abiotic factors

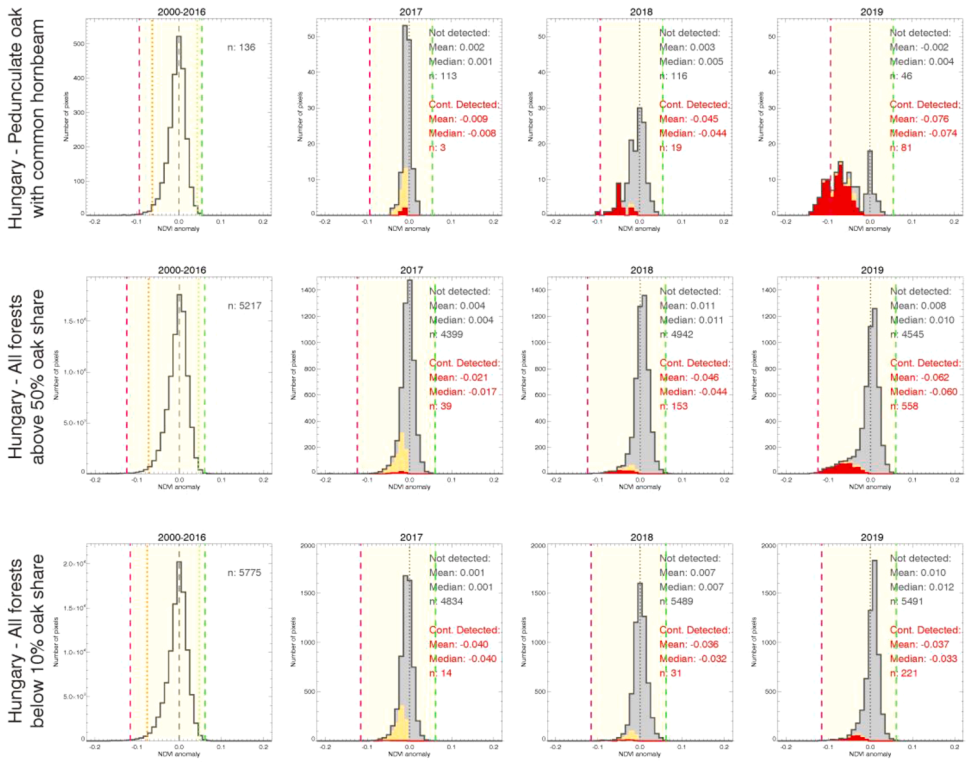

Fig. 4. Distributions of the $NDVI_{30-32}$ anomalies showing the progression of the OLB infestation detected continuously (red) or intermittently (orange) in the forest categories *Pedunculate oak with common hornbeam* (top row), *Oaks above 50% share* (middle row), and *Oaks below 10% share* (bottom row) for the Hungarian part of the study area. (For interpretation of the references to color in this figure legend, the reader is referred to the web version of this article.)

also significantly contributed to the decrease. Figs. 4 and 5 show the $NDVI_{30-32}$ anomaly distributions (grey) by years during the *OLB-era* for three main species groups in Hungary and Croatia, respectively. The $NDVI_{30-32}$ anomaly distribution during the *PreOLB-era* is shown in the first plot of the species groups as a reference, followed by the distributions for all years of the *OLB-era* (2016–2019 for Hungary and 2013–2019 for Croatia). Distributions of the pixels which were detected as continuously infested since the first year of detection (C-flag 3), and those detected intermittently (C-flag 2), are indicated separately with red and yellow colour, respectively. Dashed and dotted lines indicate the 0.1 and 1 percentile range of the overall $NDVI_{30-32}$ distribution during the *PreOLB-era*. In the lack of the *Pure pedunculate oak* category in Hungary, the *Pedunculate oak with common hornbeam* group is shown, as it is the one with the highest share of pedunculate oak. Histograms of the other species groups are presented in Figs. S4 and S5 in the Supplementary Material.

From the NDVI anomaly distributions (Figs. 4 and 5) it is visible that in the case of the forests with a significant share of oaks species the distribution started to shift toward the left into the negative anomaly range with time. The start of the observed shifts occurred approximately one year after the OLB has been found *in situ* for the first time in the study area. The magnitude of the observed anomalies is more pronounced (left of 0.1 percentile of the *PreOLB-era*) for the forest categories having the largest oak share, but not observed for the forests with less than 10% oak share. In the third year, an obvious second peak of the anomaly distribution appeared which became more and more pronounced with the spread of the OLB during the years. While in the Hungarian part of the study area the OLB infestation started in 2017, in Croatia it caused serious infestation already in 2016, with a maximum $NDVI_{30-32}$ anomaly of -0.124 for *Pure pedunculate oak* forests recorded in 2018. The control group *Oaks below 10%* share showed less interannual variability in distribution. Although there were some detected pixels with OLB-like disturbance, the $NDVI_{30-32}$ anomaly distributions showed no shifts in distribution during the *OLB-era*.

The $NDVI_{30-32}$ values of the detected pixels were affected by the OLB and at the same time by the weather and environmental conditions. The true effects of the OLB are clearer in "good years" (from the perspective of the effect of the meteorology on the vegetation state; see Kern et al., 2017; Anić et al., 2018) when the overall NDVI anomaly is positive, as was the case in Croatia (Fig. 5). There, the pixels identified as not infested in 2015 (and to a lesser extent in 2016) showed a strong overall positive anomaly, but those detected as infested showed strong negative anomaly. Similar could be observed in 2019 in the case of Hungary (Fig. 4). An interesting year is 2017, which may be characterized as a "bad year" for oak forests in Croatia since even the not detected pixels exhibited negative anomaly. There we can see a relatively higher amount of not continuously detected pixels (C-flag 2, shown in orange in Fig. 5). Moreover, we can observe a slight increase of the not continuously detected pixels in the control group as well (*Oaks below 10%* share, Fig. 5), which could be an indicator of the increased uncertainty in the ability of the RS identification method in "bad years".

Fig. 6a and b show the mean NDVI curves (trajectories) of the detected pixels with C-flag 3 in each year in the case of the *Pure pedunculate oak with common hornbeam* of Hungary and the *Pure pedunculate oak* category of Croatia, respectively, relative to the multiannual mean NDVI curves during the corresponding *PreOLB-eras*. The seasonal NDVI decrease in late summer and early autumn is obvious after the OLB was found *in situ* for the first time. Both the presented NDVI anomaly histograms (Figs. 4 and 5) and the mean NDVI curves (Fig. 6) indicates that from the time when the OLB arrives to an area it takes approximately 2–3 years for the NDVI decrease to reach its maximum, after which, it seems that it does not decrease further.

3.2. Modelling $NDVI_{30-32}$

The created models were built for the *Oaks above 20% share* forest group, separately for each country, for reasons of simplicity and robustness. The aim was to create a method that could be generally

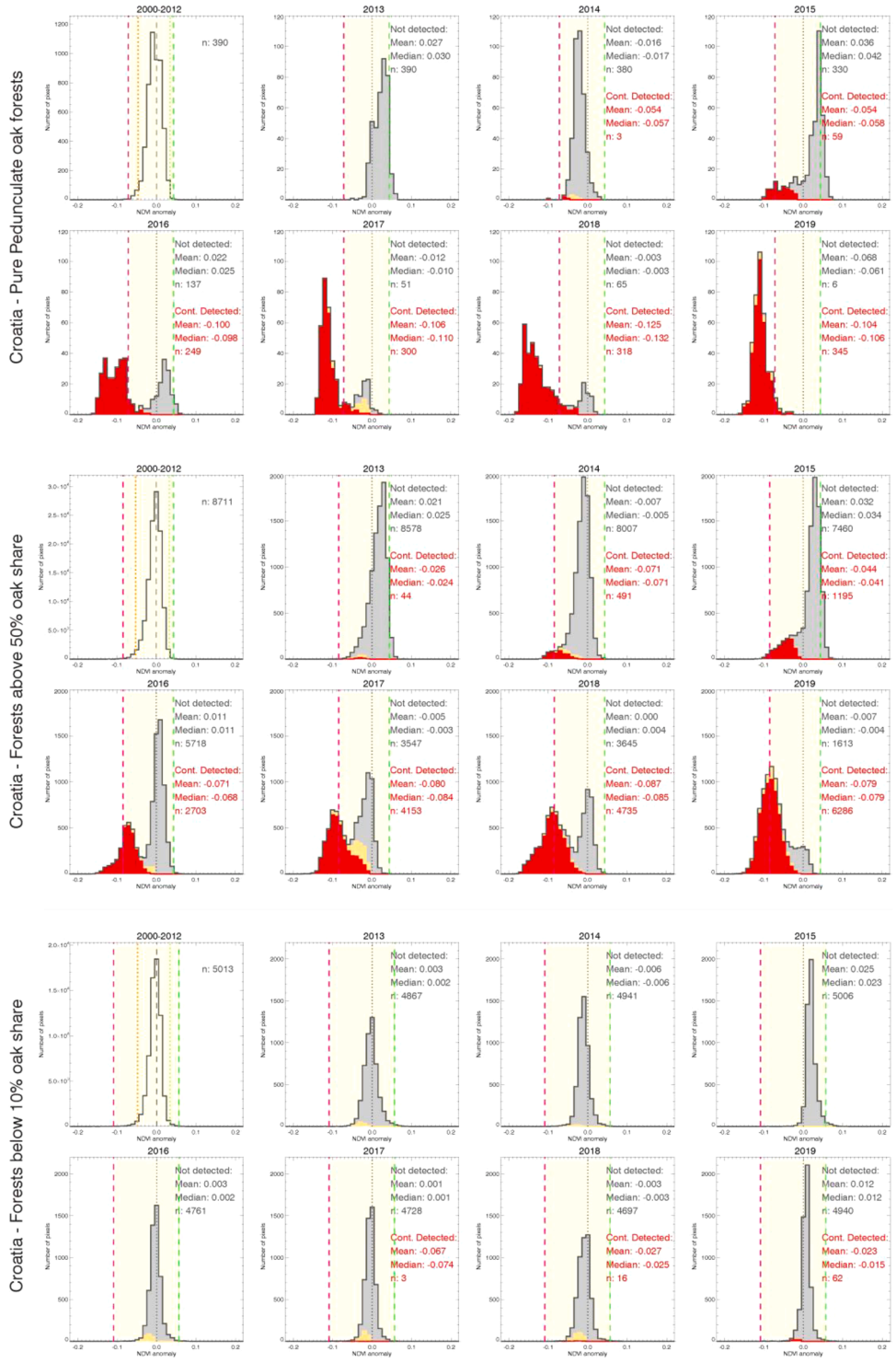

Fig. 5. Distributions of the $NDVI_{30–32}$ anomalies showing the progression of the OLB infestation detected continuously (red) or intermittently (orange) in the forest categories *Pure pedunculate oak* (top row), *Oaks above 50% share* (middle row), and *Oaks below 10% share* (bottom row) for the Croatian part of the study area. (For interpretation of the references to color in this figure legend, the reader is referred to the web version of this article.)

applied and easily reproduced, also because the tree species distribution is rarely available with a high spatial and accurate temporal resolution. The equations of the created *Lasso* models (M1 for the Hungarian and M2 for the Croatian part of the study area) are shown in Table 3. The statistics of the model coefficients (estimates, standard errors, *t*-statistics, *p*-values) are presented in Table S2 in the Supplementary Material. The parameters of the presented models were found to be significant at $p < 0.0001$ level.

After building a country-specific model for each country, the same models with the same coefficients of the linear regression were applied to the separate forest groups. Table 4 shows the performance metrics of the $NDVI_{30–32}$ models M1 and M2, during the *PreOLB-era*, which have been calibrated using the data for pixels in the *Oaks above 20% share* category and then cross-validated on the different forest groups of Hungary and Croatia, separately. Based on the calibration, the Hungarian M1 model showed an R^2 of 0.5569 with 0.0186 *RMSE*, 0.0137

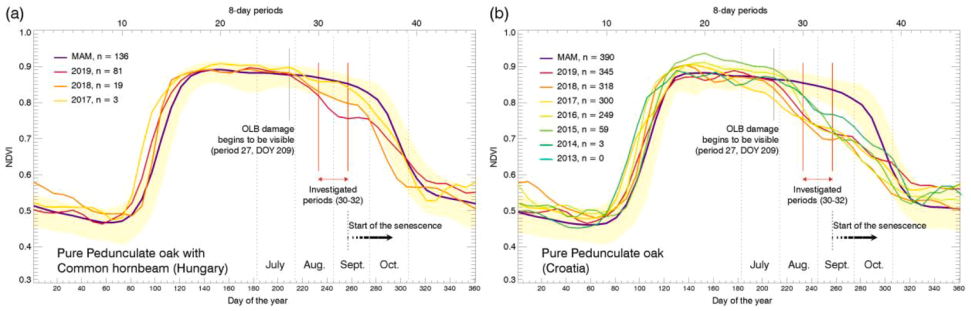

Fig. 6. Multiannual mean (*MAM*) and yearly mean NDVI curves of the detected pixels with C-flag 3 for the *Pedunculate oak with common hornbeam* category of Hungary (a) and the *Pure pedunculate oak* category of Croatia (b), where the MAM is based on 2000–2016 and 2000–2012, respectively. The range created from the average of the absolute minimum and maximum NDVI of each pixel in each period during the *PreOLB-era* is also indicated with light yellow shading (where averaging is over 136 and 390 pixels, respectively for the two countries). (For interpretation of the references to color in this figure legend, the reader is referred to the web version of this article.)

Table 3
Equations of the constructed *Lasso* models (M1 and M2) of forest $NDVI_{30–32}$ calibrated with the data of the *PreOLB-era* (2000–2012/16) for the Hungarian and Croatian part of the study area, separately. (Subscripts denote MODIS 8-day periods; see Table S3 in the Supplementary Material).

Model	Equation of the model
For Hungary	
$M1_{2000–2016}$	$NDVI_{30–32} = 0.000911 \cdot Tmax_{5–6} - 0.001891 \cdot Tmax_{21–22} + 0.004270 \cdot Tmin_{25–26} - 0.002732 \cdot Tmin_{27–28} + 0.000310 \cdot Prec_{29–30} + 0.029755 \cdot SWC3_{1–2} + 0.679711 \cdot NDVI_{25–26} + 0.269$
For Croatia	
$M2_{2000–2012}$	$NDVI_{30–32} = - 0.001115 \cdot Tmin_{1–2} - 0.002101 \cdot Tmin_{9–10} + 0.000201 \cdot Prec_{1–2} + 0.000312 \cdot Prec_{9–10} - 0.099536 \cdot SWC3_{1–2} - 0.245620 \cdot SWC3_{7–8} + 0.089088 \cdot SWC3_{29–30} + 0.267042 \cdot SWC4_{29–30} + 0.766556 \cdot NDVI_{25–26} + 0.198$

MAE, and 0.0000 *bias*, while the Croatian M2 model had an R^2 of 0.6912 with 0.0136 *RMSE*, 0.010 *MAE*, and 0.0000 *bias*. In the case of Hungary, the results of cross-validation based on the 2000–2016 *PreOLB-era* show 0.44–0.50 cross-validated R^2 values with an *RMSE* between 0.017 and 0.020. Amongst the pure forest groups, the best model performance was observed in the case of *Sessile oak with common hornbeam* group, while the poorest in the case of the pedunculate oak-dominated groups. In the case of Croatia, the cross-validated *R*-values were in the range of 0.66–0.82, with *RMSE* values between 0.011 and 0.016. The results show an unequivocally better model performance of the Croatian model than the model for Hungary.

3.3. Detecting pixels with OLB-like damage based on the MR method

In every year of the *OLB-era*, all pixels have been categorized into infested or not infested based on the *Z-score* of the model residual (see Section 2.7.2). The share of pixels identified as damaged with the *MR* method during the *PreOLB-era* on the modelling dataset (*Oaks above 20% share*) ranges from 0% to 0.79% with the mean (std. err.) of 0.12% (0.05%) in the case of Hungary. In the case of Croatia, the range was from 0% to 0.18% with the mean (std. err.) of 0.05% (0.02%). Those values represent the independent estimate of the expected share of false-positive detections with the *MR* method. The obtained shares are in line with the theoretical value for the expected false-positive OLB-detection, which is 0.1%, based on the selected *Z-score* threshold (Section 2.7.2, z = -3.09).

Fig. 7 shows the temporal evolution of the *Z-score* distributions with respect to the relative years of detection in the case of the *Oaks above 20% share* forest group, separately for Hungary and Croatia. The distribution of the *Z-score* values for the relative year of detection of -1 (one year prior to detection) is in both cases centred almost at zero and similar to the *Z-score* distributions of the previous years. This is a strong indicator that, with the selected z = -3.09 threshold the number of false-negative detections could be considered negligible.

Fig. 8 shows the yearly distributions of the model residuals (i.e. the observed NDVI - modelled NDVI) for the same species groups as in Figs. 4 and 5, with the box-whisks plot indicating the yearly mean, 1, 5, 25, 50, 75, 95 and 99 percentile values. It should be emphasized that the distributions in the *PreOLB-era* shown in Fig. 8 correspond to the distribution of the residuals in model validation. Box-plots of the pixels

Table 4
The metrics of the cross-validation performance of the $NDVI_{30–32}$ models, calibrated with the *Oaks above 20% share* category data, for different species groups of Hungary and Croatia during the corresponding *PreOLB-era*. (For the structure of the constructed model see Table 3). *N* denotes the number of the data as the number of the pixels multiplied by the number of years in the corresponding *PreOLB-era*.

Model / Species groups	*N*	R_{cv}	R^2_{cv}	P_{cv}	$RMSE_{cv}$	MAE_{cv}	$Bias_{cv}$
For Hungary ($M1_{2000–2016}$)							
Pedunculate oak with common hornbeam	2312	0.6672	0.4451	0.0000	0.0180	0.0138	0.0000
Pedunculate oak with narrow-leaved ash	2550	0.6761	0.4571	0.0000	0.0182	0.0143	-0.0003
Sessile oak with common hornbeam	8347	0.6936	0.4811	0.0000	0.0175	0.0135	-0.0026
Turkey oak	8092	0.6865	0.4713	0.0000	0.0204	0.0153	-0.0008
Pedunculate oak	7514	0.6718	0.4513	0.0000	0.0189	0.0144	0.0002
All oaks	34,816	0.7066	0.4993	0.0000	0.0196	0.0146	-0.0007
Oaks above 50% share	88,689	0.7092	0.5029	0.0000	0.0198	0.0147	-0.0002
Oaks above 20% share	**127,245**	**0.7139**	**0.5097**	**0.0000**	**0.0198**	**0.0148**	**0.0000**
Oaks below 10% share	98,175	0.7358	0.5415	0.0000	0.0204	0.0153	0.0011
For Croatia ($M2_{2000–2012}$)							
Pure Pedunculate oak	5070	0.7002	0.4903	0.0000	0.0148	0.0113	0.0015
Pedunculate oak with narrow-leaved ash	19,071	0.6979	0.4870	0.0000	0.0139	0.0108	-0.0002
Pedunculate oak with common hornbeam	20,878	0.6618	0.4380	0.0000	0.0156	0.0120	0.0009
Sessile oak with common hornbeam	1703	0.7366	0.5426	0.0000	0.0112	0.0086	0.0000
Sessile oak with common beech	15,795	0.7708	0.5941	0.0000	0.0125	0.0086	0.0000
Oaks above 50% share	113,243	0.8018	0.6429	0.0000	0.0143	0.0106	0.0006
Oaks above 20% share	**221,169**	**0.8187**	**0.6703**	**0.0000**	**0.0141**	**0.0103**	**0.0002**
Oaks below 10% share	65,169	0.8429	0.7105	0.0000	0.0164	0.0109	0.0002

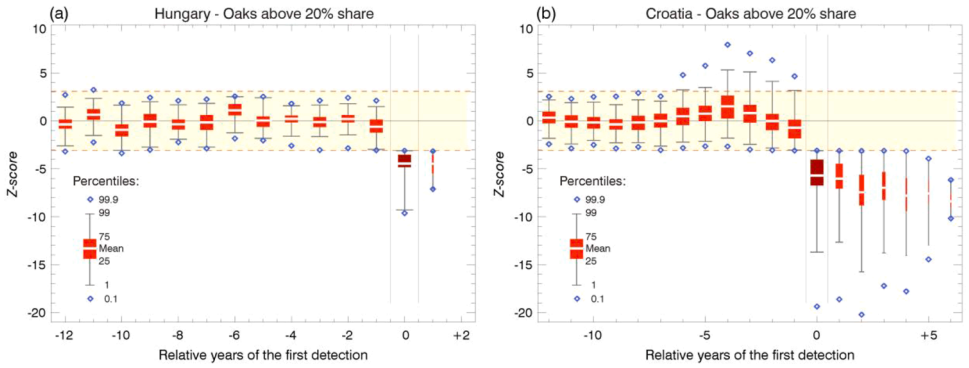

Fig. 7. Boxplots of the temporal evolution of the *Z-score* distributions of the pixels detected by the *MR* method for the first time in any year during the *PreOLB-era* in the case of *Oaks above 20% share* forest group separately for Hungary (a), and Croatia (b). Pixels detected for the first time are forming the *Z-score* distributions in the 0th year. The widths of the boxplots are reflecting the number of pixels in each of the relative years.

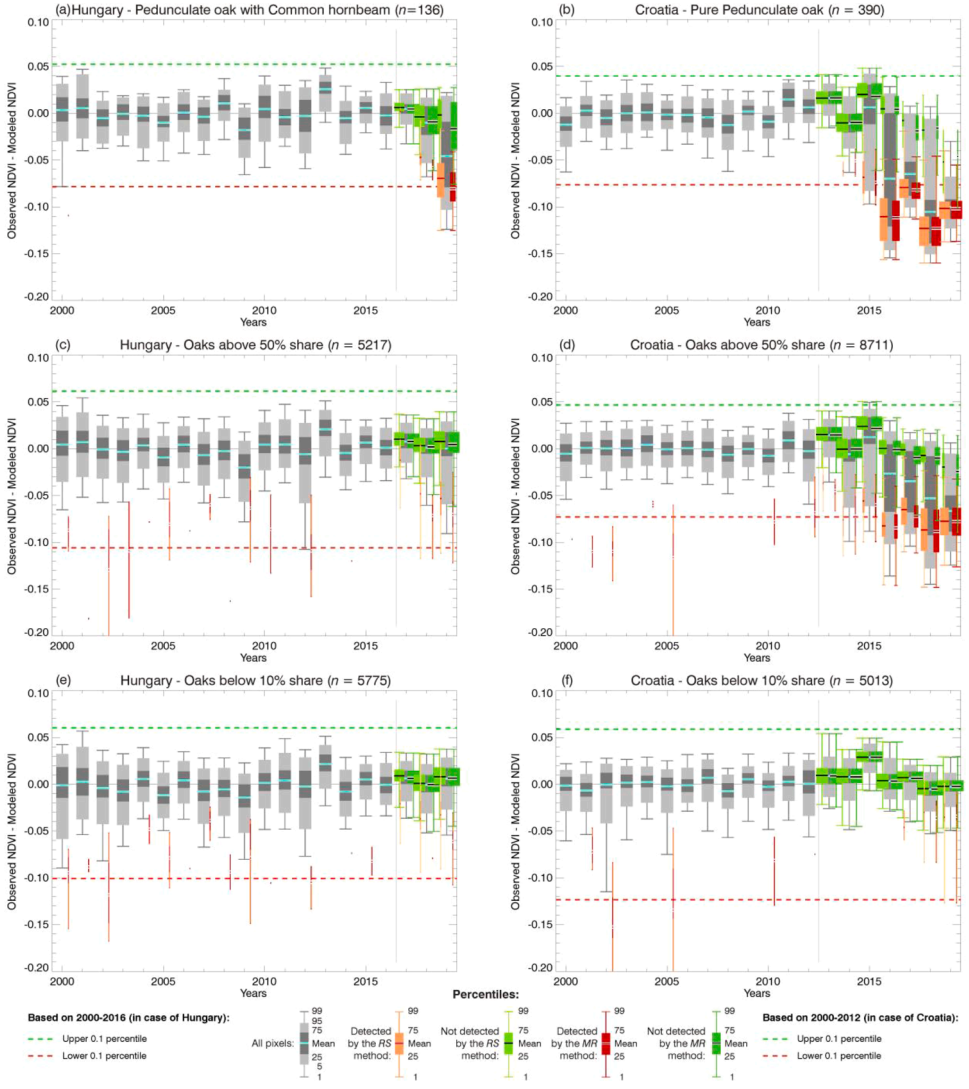

Fig. 8. Box-whisker plots of the yearly model residuals for *Pure pedunculate oak (and with common hornbeam), Oaks above 50% share*, and *Oaks below 10% share* category groups separately for Hungary (*a, c, e*) and Croatia (*b, d, f*).

detected by the *MR* method are also shown with dark red colour, throughout the entire 2000–2019 study period, where only the continuously detected pixels (i.e. with C-flag 3) are presented after 2013. During the *OLB-era* additional box-plots show separately the residual distributions of the detected (orange) and not detected (green) pixels identified by the *RS* method (with C-flag 3), where the width of the boxplots indicates the share of the pixels. The overall 1 and 0.1 percentile values (calculated separately for the different forest categories during the *PreOLB-eras*) are also shown as a reference with dotted and dashed lines, respectively.

From the presented residual distributions it is evident that the disturbance affecting the forests with oak species in the study area did not occur before the *OLB-era*. The distributions of the residuals of the *Oaks above 50% share* during the calibration (i.e. *PreOLB-era*) are mostly narrow and located around zero in every year (except 2012, which might be the lagged effect of the previous year with the extremely low precipitation in the region). Starting with 2018 (Hungary) and 2014 (Croatia) the distributions become wider and start shifting in the negative direction and away from the distribution range of the *PreOLB-era*. Not surprisingly, the largest shares of the detected OLB pixels are in forest categories with the highest oaks share (Fig. 8, top row). The control groups of the *Oaks below 10% share* showed no significant amount of pixels with negative residuals during the *OLB-era*, where the residual distributions were continuously centred near zero.

3.4. Quantification of the NDVI decrease caused by the OLB based on model residuals

The damage attributed to the OLB was estimated using the Eq. (8) (see Section 2.8), separately for the pixels detected by RS and MR methods. The descriptive statistics of the OLB caused $NDVI_{30–32}$ decrease in the Hungarian and Croatian parts of the study area are given in Table 5, separately for the only continuously (C-flag 3) and all the detected pixels (C-flag 2 or 3).

The strongest $NDVI_{30–32}$ decrease in the Hungarian part of the study area was recorded in 2019 for the *Pedunculate oak with common hornbeam* category with the mean ± std. err. of -0.070 ± 0.004 (*RS* method) and -0.081 ± 0.003 (*MR* method), corresponding to -8.1% and -9.4% relative decrease in NDVI of the infested pixels, respectively. In the case of the *Oaks above 20% share* category, the mean $NDVI_{30–32}$ decrease in the same year is smaller in magnitude, most likely due to the comparatively smaller share of oaks in that category. It is important to notice that by 2019 still only a small share of the pixels, namely 4.4% (*MR* method) and 9.1% (*RS* method) was identified as infested in that category.

In the Croatian part of the study area, the strongest recorded $NDVI_{30–32}$ decrease was in the *Pure pedunculate oak* stands in 2018 with a mean ± std. err. of -0.123 ± 0.003 (*RS* and *MR* methods), corresponding to a mean relative decrease of -14.5%. The detected share of OLB infested pixels in that category reached 88.5%–98.5% (depending on the detection method) of the area by 2019. Similarly to Hungary, in 2019 the forests category *Oaks above 20% share* exhibited a smaller magnitude of $NDVI_{30–32}$ decrease of -0.070 (both *MR* and *RS* method), while the maximum recorded mean decrease occurred in 2016 and was between -0.079 and -0.083 (depending on the method).

When comparing the results of the *RS* and *MR* methods with respect to detection continuity (C-flag 2 vs. C-flag 2 or 3), the *MR* method appears to be slightly more consistent (Table 5). Differences between the continuously and not continuously detected pixels are also present in the number of detected pixels. In the Croatian part, 88.5–91.3% of the pixels in the *Pure pedunculate oak* category were infested with the OLB by 2019. The sudden increase in the share of the infested areas (from 15.1% to 63.9%, and from 12.3% to 60.2% based on the *RS* and *MR* methods, respectively) in the *Pure pedunculate oak* category from 2015 to 2016 is striking. Considering forests above 20% oak share, the yearly increases of the detected pixels were more moderate after 2015, with an 11.6% and 12.9% share yearly increase for the *RS* and *MR* methods, respectively.

3.5. Comparison of the RS and MR method for detection of the OLB infested pixels

The difference between the *RS* and *MR* detection methods was tested using McNemar's test (McNemar, 1947). A statistically significant difference ($p < 0.0001$) was found between the two methods, both for the Hungarian and for the Croatian part of the study area, where all data were taken into account. However, the difference is not excessive and the overall agreement in detection is 91.1% in the Hungarian and 92.9% in the Croatian part (Table 6). The exception was the year 2017 in the Hungarian part when the *RS* method (C-flag 2 or 3) for the category *Oaks above 20% share* identified 1173 pixels as OLB infested, while the *MR* method identified only 13 pixels (see Table 5). In 2017 a similar case was also found in Croatia, although less drastic, with 7214 vs. 4140 pixels detected with the *RS* and *MR* methods, respectively (Table 5).

The continuity of detection was investigated by looking into the statuses of the infestation in the current year for the pixels that had been identified as infested in the previous year by the *RS* or *MR* method. The results in Table 6 show a very good overall agreement between *RS* and *MR* methods, ranging from 83.6% to 94.4%. The effects of 2017 are again visible from the performance of the *RS* method in the case of Hungary. Tables S4 and S5 in the Supplementary Material show the comparison at the yearly level, separately for Hungary and Croatia.

3.6. Relationship between the model residuals and the oaks-share

Having at our disposal data on wood volume for all tree species present within each Croatian pixel, we investigated the relationship between the magnitude of the model residuals and the share of oaks during the *OLB-era*. The scatter plots of the yearly $NDVI_{30–32}$ residuals versus the total share of all oak species in the *Oaks above 20% share* category are presented in Fig. 9 for the Croatian part of the study area. The pixels identified by the *RS* method and the *MR* method are indicated with orange and red, respectively. Only pixels with C-flag 3 were used to ensure the highest reliability of OLB detection. Pearson *R* and the equation of the linear regression line are also shown when significant ($p < 0.01$), namely from 2014.

The slope of the regression line for the detected pixels is always significantly ($p < 0.0001$) negative, ranging from -0.074 to -0.127 (*RS* method) and -0.056 to -0.124 (*MR* method), reflecting the fact that the residuals of the $NDVI_{30–32}$ model decrease with increasing oak share in the pixels. This is an indicator that the observed $NDVI_{30–32}$ decrease is primarily due to some detrimental effect on oak trees, which is known from the field observation to be caused by the strong OLB infestation.

Even though the *RS* method generally tends to identify more pixels than the *MR* method, Fig. 9 shows that the identification of the infested pixels by both methods are in very good agreement, resulting in very similar equations in each year. The most contrasting year is again 2017 (see Section 3.5) when the *RS* method detected more OLB-infested pixels. The *RS* method detected more pixels with a smaller share of oaks and relatively small negative residuals, resulting in a steeper regression line.

The not infested pixels are also exhibiting statistically significant and slightly negative slopes ($p < 0.0001$), although the magnitudes are small in comparison with the slopes of the infested ones. The slope for the non-infested pixels is most negative in 2014 and to a lesser degree in 2015 when the OLB started to spread after its establishment in the Spačva forest in Croatia in 2013. Here it is worth pointing out the noticeably positive residual of the not-infested pixels in 2015 when coincidentally some of the pixels near the origin of infestation were not detected (with *MR* C-flag 3), although they have been detected as infested in both 2013 and 2014.

3.7. The detected spread of the OLB damage

Fig. 10a and b show the maps of the detected OLB spread based on the continuously detected pixels (C-flag 3) of the study area, determined by both *RS* and *MR* methods, respectively. In line with our methodology, the maps show only pixels with forest area share above 95%. This means that the map of the OLB spread does not indicate all the areas where OLB is present, but it does provide information on the geographical spread of the pest with time.

Pixels, which had a break in the continuity of the detection during

Table 5
Descriptive statistics (pixel number, mean ± std. err., relative decrease) of the estimated yearly $NDVI_{30-32}$ decrease attributed to the OLB in the study area for the pixels continuously (C-flag 2) and at any time (C-flag 2 or 3) detected as OLB infested using the *RS* and *MR* method. For brevity, only results for the forest categories with the highest and oak share and for the largest category *Oak above 20% share* are presented.

Country (PreOLB-era) Species groups & PreOLB $NDVI_{30-32}$ (n_{pixels}; $\bar{x} \pm s.e.$)	Year	Pixels detected by the RS method (with C-flag 3) n (share)	 mean NDVI decrease ($\bar{D}_{30-32,\ y}$)	 mean relative decrease	Pixels detected by the RS method (with C-flag 2 or 3) n (share)	 mean NDVI decrease ($\bar{D}_{30-32,\ y}$)	 mean relative decrease	Pixels detected by the MR method (with C-flag 3) n (share)	 mean NDVI decrease ($\bar{D}_{30-32,\ y}$)	 mean relative decrease	Pixels detected by the MR method (with C-flag 2 or 3) n (share)	 mean NDVI decrease ($\bar{D}_{30-32,\ y}$)	 mean relative decrease
Hungary (2000–2016)													
Pedunculate oak with common hornbeam (136; 0.861 ±0.024)	2017	3 (2.2%)	0.002 ± 0.003	0.2%	23 (16.9%)	-0.004 ± 0.004	-0.4%	0 (0%)	-	-	0 (0%)	-	-
	2018	19 (14.0%)	-0.047 ± 0.004	-5.5%	20 (14.7%)	-0.047 ± 0.004	-5.4%	3 (2.2%)	-0.058 ± 0.007	-6.8%	3 (2.2%)	-0.058 ± 0.007	-6.8%
	2019	81 (59.6%)	**-0.070** ± 0.004	**-8.1%**	90 (66.2%)	**-0.068** ± 0.004	**-7.9%**	62 (45.6%)	**-0.081** ± 0.003	**-9.4%**	62 (45.6%)	**-0.081** ± 0.003	**-9.4%**
Oaks above 20% share (7485; 0.861 ± 0.028)	2017	48 (0.6%)	-0.011 ± 0.003	-1.3%	1173 (15.7%)	-0.006 ± 0.002	-0.7%	0 (0%)	-	-	13 (0.2%)	-0.060 ± 0.012	-7.0%
	2018	175 (2.3%)	-0.048 ± 0.003	-5.5%	369 (4.9%)	-0.036 ± 0.003	-4.1%	41 (0.6%)	**-0.071** ± 0.003	**-8.3%**	60 (0.8%)	**-0.071** ± 0.003	**-8.3%**
	2019	683 (9.1%)	**-0.050** ± 0.002	**-5.8%**	835 (11.2%)	**-0.049** ± 0.002	-5.6%	330 (4.4%)	-0.069 ± 0.002	-8.1%	330 (4.4%)	-0.069 ± 0.002	-8.1%
Croatia (2000–2012)													
Pure pedunculate oak (390; 0.849 ± 0.021)	2013	0 (0%)	-	-	0 (0%)	-	-	0 (0%)	-	-	1 (0.3%)	-0.040	-4.7%
	2014	3 (0.8%)	-0.062 ± 0.005	-7.3%	10 (2.6%)	-0.042 ± 0.009	-4.9%	7 (1.8%)	-0.051 ± 0.005	-6.0%	13 (3.3%)	-0.050 ± 0.005	-5.9%
	2015	59 (15.1%)	-0.068 ± 0.003	-8.1%	60 (15.4%)	-0.069 ± 0.003	-8.2%	48 (12.3%)	-0.074 ± 0.003	-8.7%	49 (12.6%)	-0.075 ± 0.003	-8.8%
	2016	249 (63.9%)	-0.110 ± 0.003	-13.0%	253 (64.9%)	-0.110 ± 0.003	-13.0%	235 (60.2%)	-0.112 ± 0.003	-13.2%	252 (64.6%)	-0.111 ± 0.003	-13.0%
	2017	300 (76.9%)	-0.079 ± 0.002	-9.4%	339 (86.9%)	-0.074 ± 0.003	-8.7%	278 (71.3%)	-0.082 ± 0.002	-9.7%	288 (73.9%)	-0.081 ± 0.002	-9.6%
	2018	318 (81.6%)	**-0.123** ± 0.003	**-14.5%**	325 (83.3%)	**-0.123** ± 0.003	**-14.5%**	307 (78.7%)	**-0.123** ± 0.003	**-14.5%**	329 (84.4%)	**-0.122** ± 0.003	**-14.4%**
	2019	345 (88.5%)	-0.102 ± 0.002	-12.0%	384 (98.5%)	-0.101 ± 0.002	-11.9%	356 (91.3%)	-0.102 ± 0.002	-12.0%	379 (97.2%)	-0.102 ± 0.002	-12.0%
Oaks above 20% share (17013; 0.863 ± 0.025)	2013	45 (0.3%)	-0.037 ± 0.002	-4.3%	198 (1.2%)	-0.032 ± 0.002	-3.7%	23 (0.1%)	-0.045 ± 0.002	-5.2%	72 (0.4%)	-0.050 ± 0.003	-5.8%
	2014	517 (3.0%)	-0.075 ± 0.002	-8.7%	849 (5.0%)	-0.060 ± 0.002	-6.9%	491 (2.9%)	-0.072 ± 0.002	-8.3%	786 (4.6%)	-0.068 ± 0.001	-7.8%
	2015	1330 (7.8%)	-0.054 ± 0.001	-6.2%	1414 (8.3%)	-0.053 ± 0.001	-6.2%	965 (5.7%)	-0.059 ± 0.001	-6.9%	1024 (6.0%)	-0.060 ± 0.001	-7.0%
	2016	3043 (17.9%)	**-0.079** ± 0.001	**-9.2%**	3753 (22.1%)	-0.070 ± 0.001	-8.1%	2577 (15.2%)	**-0.083** ± 0.001	**-9.6%**	3093 (18.2%)	-0.080 ± 0.001	-9.2%
	2017	5218 (30.7%)	-0.060 ± 0.001	-7.0%	7214 (42.4%)	-0.050 ± 0.001	-5.8%	3608 (21.2%)	-0.070 ± 0.001	-8.1%	4140 (24.3%)	-0.069 ± 0.001	-8.0%
	2018	6378 (37.5%)	-0.078 ± 0.001	-9.0%	7331 (43.1%)	**-0.074** ± 0.001	**-8.6%**	5364 (31.5%)	-0.081 ± 0.001	-9.4%	6339 (37.3%)	**-0.080** ± 0.001	**-9.3%**
	2019	9193 (54.0%)	-0.070 ± 0.001	-8.1%	10603 (62.3%)	-0.070 ± 0.001	-8.1%	9715 (57.1%)	-0.070 ± 0.001	-8.1%	10312 (60.6%)	-0.070 ± 0.001	-8.1%

Table 6
Comparison of the *RS* and *MR* methods for detection of the OLB infestation and of the continuity in detection. (0 – not infested; 1 – infested; e.g. RS1_MR1 - infestation detected with both methods).

Case / Country	*RS1 & MR1*	*RS0 & MR1*	*RS1 & MR0*	*RS0 & MR0*	*RS & MR* in agreement
OLB infestation detection with RS and MR methods for the OLB-era					
Hungary	394 (1.8%)	9 (0.0%)	1,983 (8.8%)	20,069 (89.4%)	91.1%
Croatia	24,350 (20.4%)	1,416 (1.2%)	7,012 (5.9%)	86,313 (72.5%)	92.9%
*CURRENT year status of pixels detected with **RS** as infested in the PREVIOUS year*					
Hungary	121 (7.8%)	0 (0.0%)	143 (9.3%)	1,278 (82.9%)	90.7%
Croatia	15,974 (76.9%)	240 (1.2%)	1,753 (8.4%)	2,792 (13.4%)	90.4%
*CURRENT year status of pixels detected with **MR** as infested in the PREVIOUS year*					
Hungary	42 (57.5%)	0 (0.0%)	12 (16.4%)	19 (26.0%)	83.6%
Croatia	14,058 (91.0%)	184 (1.2%)	678 (4.4%)	534 (3.5%)	94.4%

the *OLB-era* are in Hungary mostly those of the *Sessile oak* forest group in the mountainous area, while in Croatia they are from *the Pedunculate oak with common hornbeam* or *Pedunculate oak with narrow-leaved ash* forest groups. As it can be seen from the maps, the initial origin of the OLB infestation in the study area was in the Spačva forest in Croatia (Fig. 10a and b, Southeast corner) in 2013. The pixels which are shown with blue in Fig. 10a and b (as not continuously detected) were detected in 2013, 2014, and 2016, but not in 2015. The year 2015 was the year when the model had a positive bias, indicating that 2015 was a "good year" and both *RS* and *MR* under-performed, causing a break in the continuity of detection (see Section 3.6, Fig. 10).

Fig. 11 presents the magnified maps of the detected OLB spread in the Spačva forest, where the year of the first detection was shown regardless of the temporal continuity of the detection (i.e. C-flag 2 or 3) based on both detection methods.

Both the *RS* and *MR* methods are in good agreement (within 1 km) regarding the possible location of the origin of the OLB infestation in the study area. According to our study, the estimated origin (centroid of all four locations, identified with *RS* and *MR* methods and two C-flags – see Fig. 11) was the location with coordinates of 45.034°N and 19.004°E. This location is approximately 1 km south of the gas station and resting place with a hotel and a camp on a highway. The resting place is near the border crossing between Croatia (EU) and Serbia and it is frequently used by truck drivers and others using that highway which is part of the Pan-European Corridor X that goes from Salzburg (Austria) to Thessaloniki (Greece) or by a connection to Pan-European Corridor IV to Sofia (Bulgaria) and Istanbul (Turkey).

The radial spread (Fig. 12) and the corresponding speed of the OLB spread calculated with the *RS* (*MR*) method was slow at first, with only 1.4 (1.2) km y^{-1} in 2013 to 5.5 (5.3) km y^{-1} in 2015, but then increased dramatically with the maximum of 57.7 (55.3) km y^{-1} in 2017.

3.8. Agreement between OLB detection with RS and MR methods and in situ records

The overview of the agreement between the two detection methods and the *in situ* records of OLB presence is given in Table 7. McNemar's test confirmed that all detection results, regardless of the method, differ significantly ($p < 0.0001$) from the *in situ* records for the presence of the OLB.

The average agreement between a given detection method and the *in situ* information ranged from 71.7% (*MR*, C-flag 3) and 82.2% (*RS*, C-flag 2 or 3) in the case of Croatia for the 2016–2019 period, while it was 73.9% (*RS*, C-flag 2 or 3) and 77.0% (*MR*, C-flag 3) in the case of Hungary in 2019 (the only year when *in situ* records were available). Comparing the results between the two countries only for the year 2019, it becomes apparent that the agreement of the *in situ* records is better with the *RS* method in Croatia, but in the case of Hungary, it is better with the *MR* method. Furthermore, for Croatia, the agreement between the detected and the *in situ* records decreases with time regardless of the method.

4. Discussion

4.1. Methodological aspects

The aim of our study was to identify the infestation and to assess the damage attributed to the OLB in the transboundary area of Hungary and Croatia primarily using MODIS NDVI data. We identified the optimal period for OLB detection (21 Aug – 13 Sep) when the OLB caused NDVI decrease is already pronounced and observable by remote sensing tools, but the senescence is still not affecting the phenological curve. The identification of the infestation was made only for selected pixels of the different species groups which minimized the chance of the infestation misclassification.

Another important issue is the natural variability of the NDVI that occurs purely due to the different yearly weather and environmental conditions in the absence of the pest. The importance of such VI variability has been recognized in some of the studies on detecting pest damage (e.g. Chávez et al., 2019), but the yearly effects of the

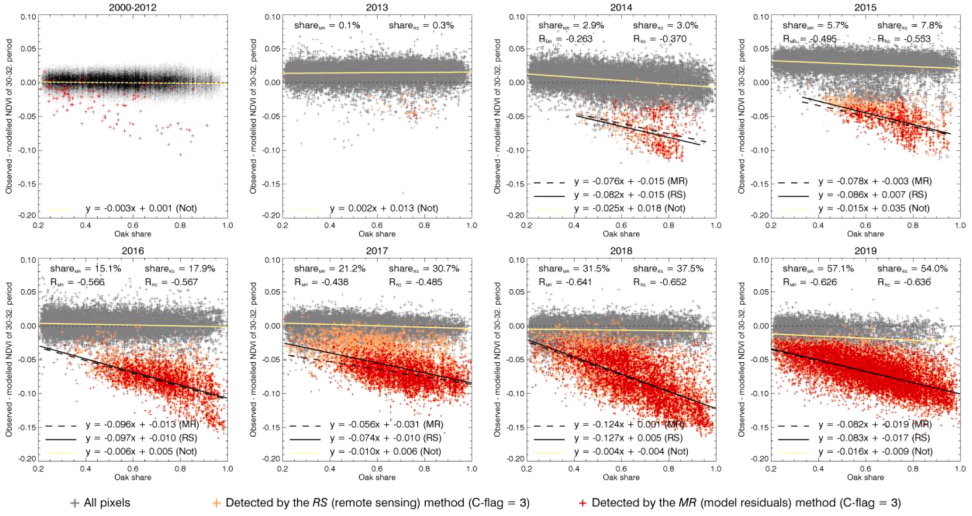

Fig. 9. Scatter plots of the $NDVI_{30–32}$ model residuals versus the oak share during the *OLB-era* (2013–2019) for the *Oaks above 20% share* category in the Croatian part of the study area by years. The first plot is the scatter plot of the overall data during the *PreOLB-era* (2000–2012), showed by a density plot (where the red pixels are the OLB false-positive detected pixels). Pixels identified as infested by the *RS* and *MR* method (with C-flag 3) are indicated with orange and red, respectively on the subsequent plots, while the not detected are in grey. The share of the detected OLB infested pixels ($share_{RS}$ & $share_{MR}$), Pearson *R*, the equations and lines of the fitted linear regressions ($p < 0.0001$) are also shown.

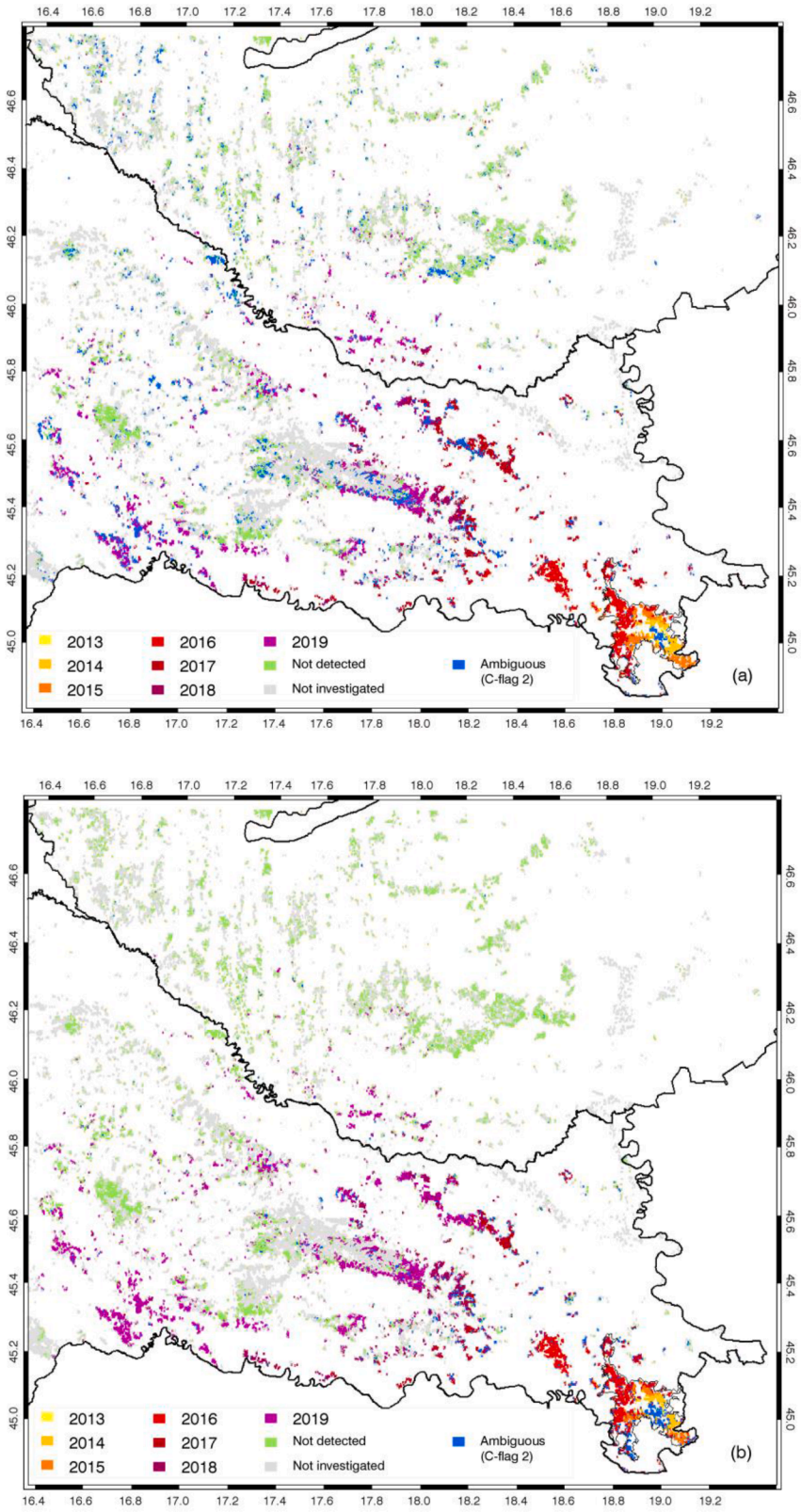

Fig. 10. Maps of the detected OLB spread in the study domain based on the year of the first detection during the 30–32th 8-day period (DOY 233–256), determined by *RS* (a) and *MR* (b) methods, respectively. In the Spačva forest (Southeastern corner) the blue (not continuously detected) pixels were detected in 2013, 2014, and 2016, but not in 2015.

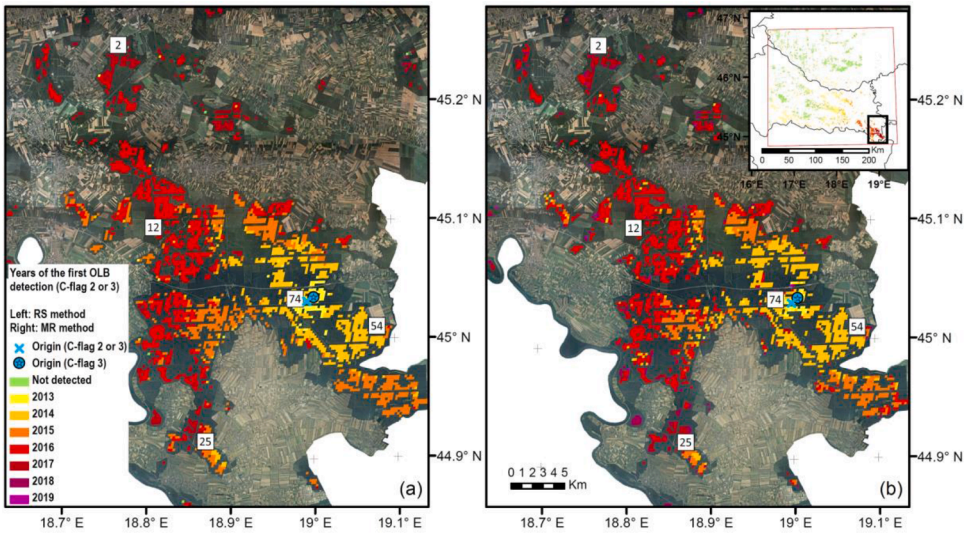

Fig. 11. Maps of the origin and the detected OLB spread in the Spačva forest (Croatia) based on the year of the first detection during the 30–32th 8-day period (DOY 233–256), determined both by the (a) *RS* and (b) *MR* method. Colours from yellow to purple are showing years independently from the C-flag. The square symbols mark the locations with the numbers of the individual OLB insects found *in situ* in 2013 by Hrašovec *et al.* (2013).

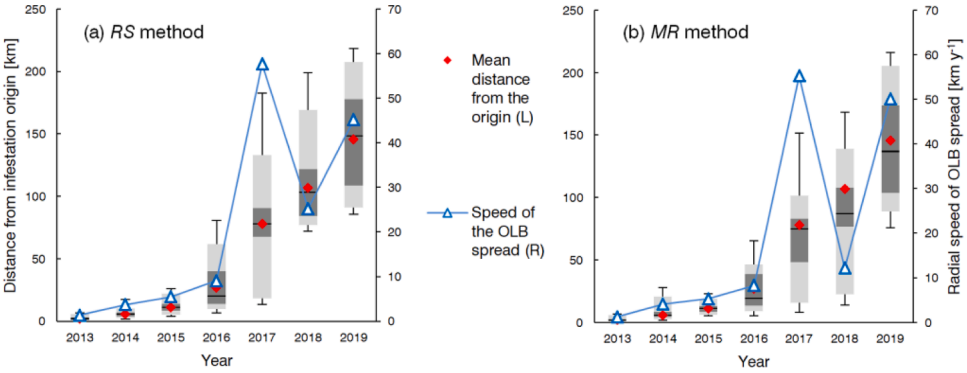

Fig. 12. Radial distance and speed of the radial spread from the infestation origin in Spačva forest during the investigated period determined by the (a) *RS* method and (b) *MR* method (whiskers: 1 and 99 percentile; light grey box: 5 and 95 p; dark grey box: 25 and 75 p; horizontal line: median distance).

meteorology or soil moisture on the used vegetation indices were generally not considered in such studies. The reasons for usually neglecting the yearly variability of the weather and soil moisture in such studies could be because the magnitude of the VI's change is typically small compared to the decrease due to pest damage, especially in the case of strong defoliation. In the case of the OLB infestation, which in some part of our study area (e.g. Spačva forest) has been lasting already for 8 years, it is necessary to take into account the NDVI variability caused by meteorological and other environmental factors. Our attempt to explicitly address the effects of the environmental variables on the NDVI by the *MR* method therefore could be considered a novelty. On the other hand, methods based on the deviation from the yearly maximum NDVI (e.g. de Beurs and Townsend, 2008; Spruce et al., 2011) indirectly account for the actual yearly weather and soil conditions. Likewise, since the presented *RS* detection method is based on the yearly NDVI difference between the current year growing season maximum NDVI and the $MeanNDVIdiff_{i,j,PreOLB}$ (see Eq. (2) & (3)), it also implies that the interannual variability in the NDVI curve has been accounted for.

During our model construction, the emphasis was on the model robustness and high statistical significance resulting in NDVI models with a relatively small number of predictor variables. The applied *Lasso* approach facilitated the selection of the smallest set of highly significant variables. The difference between the sets of selected variables (and the corresponding coefficients) in the $NDVI_{30–32}$ models indicate that the division of the study area to the Hungarian and Croatian part was justified. The models (Table 6) indicate that in the Hungarian part the $NDVI_{30–32}$ increases when the winter temperatures are milder ($Tmax_{5–6}$) and the soil moisture in the rooting zone ($SWC3_{1-2}$) is higher, the late spring is not too hot ($Tmax_{21–22}$), the temperatures in the peak summer remain high ($Tmin_{25–26}$), but not getting too high ($Tmax_{27–28}$), and with increasing precipitation in the second half of August ($Prec_{29–30}$).

Contrary to that, in the Croatian part the $NDVI_{30–32}$ increases with harsher winters ($Tmin_{1–2}$, $Tmin_{9–10}$) with more abundant precipitation ($Prec_{1–2}$, $Prec_{9-10}$), but not too high soil water content ($SWC3_{1–2}$, $SWC3_{7–8}$) which might indicate that the snow is the preferred precipitation during winter. Another important difference is related to water supply in late summer. While for the Hungarian part the $NDVI_{30–32}$ was positively influenced by the precipitation in late summer, in the Croatian part the most important late-summer variables were $SWC3_{29–30}$ and $SWC4_{29–30}$ pointing at the importance of the groundwater for the supply of trees with water.

The applied *Z-score* threshold (-3.09) is similar to the one (-2.9) used by Olsson et al. (2016a) and was selected to facilitate a conservative estimate for the presence of the OLB infestation in a pixel. Using a slightly less negative *Z-score* (e.g. the mentioned -2.9) in our study would likely improve the agreement between *MR* and *RS* methods (91.1% and 92.9% agreement for Hungary and Croatia, respectively; Table 6), but at increasing risk of a higher share of false-positive for

Table 7
Agreement shares between OLB detection with different methods and *in situ** estimate for forests in the *Oaks above 20%* category (0 – not infested; 1 – infested; e.g. 1-0 denotes the share of pixels detected as infested, while *in situ* records indicate no infestation was present).

Country	Method*	Year	OLB detected – OLB *in situ***				N	Agreement	Odds ratio 1-0 / 0-1
			1–1	1–0	0–1	0–0			
Croatia	RS_{23}	2016	0.244	0.031	0.040	0.685	12,655	92.9%	0.78
		2017	0.465	0.059	0.100	0.376	12,655	84.1%	0.59
		2018	0.498	0.044	0.216	0.242	12,655	74.0%	0.20
		2019	0.694	0.000	0.306	0.000	12,655	69.4%	0.00
		2016-2019	0.475	0.033	0.166	0.326	50,620	80.1%	0.20
	RS_3	2016	0.230	0.010	0.054	0.706	12,655	93.6%	0.18
		2017	0.391	0.013	0.174	0.422	12,655	81.3%	0.08
		2018	0.445	0.035	0.269	0.251	12,655	69.6%	0.13
		2019	0.612	0.000	0.388	0.000	12,655	61.2%	0.00
		2016-2019	0.420	0.014	0.221	0.345	50,620	76.5%	0.06
	MR_{23}	2016	0.232	0.010	0.052	0.706	12,655	93.8%	0.19
		2017	0.315	0.008	0.250	0.427	12,655	74.2%	0.03
		2018	0.446	0.030	0.268	0.255	12,655	70.2%	0.11
		2019	0.654	0.000	0.346	0.000	12,655	65.4%	0.00
		2016-2019	0.412	0.012	0.229	0.347	50,620	75.9%	0.05
	MR_3	2016	0.201	0.002	0.083	0.713	12,655	91.5%	0.03
		2017	0.280	0.005	0.285	0.430	12,655	71.0%	0.02
		2018	0.376	0.028	0.338	0.257	12,655	63.4%	0.08
		2019	0.611	0.000	0.389	0.000	12,655	61.1%	0.00
		2016-2019	0.367	0.009	0.274	0.350	50,620	71.7%	0.03
Hungary	RS_{23}	2019	0.032	0.080	0.181	0.707	7,485	73.9%	0.44
	RS_3	2019	0.026	0.065	0.187	0.722	7,485	74.8%	0.35
	MR_{23}	2019	0.014	0.030	0.199	0.757	7,485	77.0%	0.15
	MR_3	2019	0.014	0.030	0.199	0.757	7,485	77.0%	0.15
All	RS_{23}	Combined	0.171	0.060	0.173	0.375	58,105	70.1%	0.34
	RS_3	Combined	0.088	0.040	0.204	0.393	58,105	66.3%	0.20
	MR_{23}	Combined	0.116	0.021	0.214	0.400	58,105	68.7%	0.10
	MR_3	Combined	0.075	0.018	0.235	0.403	58,105	65.3%	0.08

* Numbers next to *RS* and *MR* denote the continuity of detection (23 – intermittently or continuously; 3 – continuously after the first detection; Section 2.6).
** In the case of Croatia, the *in situ* corresponds to the estimates of the OLB presence at the level of the forest management unitN – Number of pixels surveyed for the OLB (in Croatia only part of the forest area was surveyed; see Section 2.2).

infestation. The comparison with the *in situ* records offers some additional insight. In the case of Hungary, the *MR* method shows better agreement with the *in situ* than the *RS* method while for Croatia it is *vice versa*. However, in the case of both countries, the odds ratio of false-positive to false-negative detection for the *MR* method is smaller than one, indicating that the *MR* method is more likely to provide a false-negative result.

The optimal value of the *Z-score* also depends on the aim of the research. In our study, the aim was to confirm the OLB presence with high likelihood and assess the impact of the pest. Therefore, the false-positive was less desirable than the false-negative as we want to quantify the damage that is most likely the result of the OLB and not of something else. However, if the study would aim to map the outer limits of the possible spread (e.g. as support in selecting the best measures for limiting the further spread), the inverse would be true and in that case, false-negative should be minimised and the smaller magnitude *Z-score* would be suitable. The selection of the best value for *Z-score* calls for further research, in particular related to the share of oaks in a pixel where the smaller magnitude *Z-score* threshold might be more appropriate for forests with a lower share of oaks.

Nevertheless, if we consider the results from both OLB detection methods, the observed good agreement between *RS* and *MR* validates the use of the much simpler *RS* method as it provides a similar agreement with the *in situ* records.

4.2. Causes of model uncertainty

The deviations between the modelled and observed data can be due to many factors, such as: errors in the measured and processed NDVI (i.e. noises due to atmospheric and angular effects, gridding and compositing issues, geographic inaccuracies in remote sensing data); non-linearity and latency effects of the meteorology; inaccuracies in the used meteorological and soil water content data; inaccuracies in the forest maps and land cover datasets; interactions between the weather and the life cycle of the OLB; damage from other pests or diseases; abiotic disturbances; and finally, due to the model design. Considering all mentioned possible error sources the overall accuracy of the created models can be considered satisfactory. Based on the cross-validation, the models explained 44–51% and 44–67% of the observed $NDVI_{30–32}$ variability in the investigated species group of the Hungarian and Croatian study area, respectively (Table 4). Verbesselt et al. (2009) also used MODIS and daily meteorological data in their model to forecast insect-induced tree mortality, although only the long-term climate data averages were considered. They reported a similar performance of their model and found a clear improvement (from R^2 of 0.39 to 0.48) when the average temperature was included, but not for other meteorological variables.

The NDVI index is known to saturate in high-density forest areas (Huete et al., 1997). Early infestation signs in such high-density forests might be unnoticed by remotely sensed NDVI. The oak forests in our study area are managed and regular thinning is a standard management practice, thus the likelihood for the strong influence of any NDVI saturation on the OLB detection is small.

The uncertainties during our model work were also manifesting as temporal (dis)continuity of the detection in some pixels. The information on the continuity of the detection (C-flag) proved to be an important element in assessing the reliability of the OLB infestation detection, especially in years 2014 and 2017 when the not-continuously detected pixels spiked (Table 5).

Finally, the use of any model relying on meteorological data is inherently limited by the range of the meteorology used in model calibration. The use of the model for the prediction of the status of any living system in cases when the input meteorology to the model is outside of the calibration range should be avoided and all such results should be taken with caution. This is particularly the case when temperatures exceeding the maximum or precipitation (soil water content) go below the minimum of the calibration range. In such cases, the non-linear

nature of the relationship between a dependent (modelled) variable and independent (meteorological) variables might lead to increasingly erroneous results, especially in linear models such as those used in this study. Fortunately, in our case, the meteorological variables used for the prediction of the $NDVI_{30\text{-}32}$ were almost always within the calibration range (see Fig. S6 in the Supplementary Material). The one exception was the precipitation in spring 2014 (MODIS periods 6 to 17) in the case of Croatia, which exceeded the calibration range. Given that the soil was already wet, this had no significant effect on the results (see Fig. 8). However, the increasing likelihood of extreme weather (due to climate change) emphasises the limits of such models.

4.3. Importance of the land cover datasets and information on forest management

Using land cover and forest inventory datasets and selecting highly forested pixels were essential in this study. Our work was based on pixels with high (>95%) forest share during the whole study period, which was stricter than the 90% criterion applied by e.g. de Beurs and Townsend (2008), or by Eklundh et al. (2009). High forest cover in a pixel, but also in the side-neighbouring pixels (>60%), guaranteed that the observed anomaly is not likely an effect of the nearby croplands or grasslands. The importance of the land cover type of the bordering pixels was recognized in similar studies as well (e.g. Fraser et al., 2005; Eklundh et al., 2009; Olsson et al., 2016b).

There are many studies in the literature focusing on the MODIS-based detection of forest disturbances caused by e.g. harvesting or burning that could lead to changes in the land cover (Jin and Sader, 2005; Lunetta et al., 2006; Hayes et al., 2008). During our research, the emphasis was on using only those pixels which are surely free from any significant land cover and forest composition change. Similarly careful in the pixel selection were e.g. Griffiths et al. (2014), who used only those units in their study in the Carpathian ecoregion, which had an estimated stand age of at least 30 years, to ensure the unchanged forest composition in their Landsat-based disturbance detection. In our case, the effect of forest management and any significant harvesting within the pixel were taken into account both for Hungary and Croatia, although differently due to the differences in the national land cover data. In the case of Croatia, the forest management data resampled to the MODIS grid was used to exclude pixels with significant forest management during 2005–2019 (>35% total harvest intensity in the period). In the lack of similar forest management data for Hungary, only pixels with stable yearly growing season phenological curves were used (see Section 2.5.2). This criterion is similar to the one used by Lunetta et al. (2006) however, in our case, only the main part of the growing season was taken into account in the calculation of the mean NDVI. The disturbance from forest fires in the region so far has very been rare. The MODIS dataset on the burned areas (MCD64 A1) shows that fires are limited to agricultural areas (residue burning in autumn) with no forest fires during the OLB era.

Categorization of forests into different groups based on tree species composition improved the assessment of the OLB impact, but also facilitated taking into account the possible effects of other important tree diseases such as *Hymenoscyphus fraxineus* (T. Kowalski) Baral, Queloz, and Hosoya which causes ash dieback. Information on disturbances due to forest management helped the model performance and this could be one of the reasons why the modelling results were better for the Croatian part of the study area (for the *Oaks above 20% share* group the $RMSE = 0.0141$; Table 4), where forest management data was available, in comparison to modelling result for the Hungarian part (for the *Oaks above 20% share* group $RMSE = 0.0198$), where forest management data had to be inferred from the growing season phenological curve. These land cover related issues emphasized the high value of the forest type maps and existing forest management data at fine spatial resolution.

4.4. Validation issues

In the case of the Hungarian ground observation dataset, the *in situ* damage assessment and the observed NDVI data was only one year long (the year 2019), while in the case of Croatia the *in situ* assessments were made for large areas (FMU level) and were of varying precision (in different years more detailed for some FMU-s, and less so for others). Such coarseness meant that whenever the OLB was found in any part of an FMU, the whole unit was classified as infested, although some parts of it were maybe still not. This means that, in cases of some pixels in Croatia, the *in situ* status of OLB infestation could be false-positive. The declining accuracy of *MR* and *RS* detection with time could be linked with the fact that the share of oaks in the Croatian FMUs declines westward, i.e. in the direction of the OLB spread. With the widening of the area of OLB infestation the average share of oak species in the area (FMUs) where the OLB infestation has been recorded *in situ* decreased from 69.3% (2016) to 54.5% (2017) to 49.4% (2018) and finally to 43.3% (2019). The decreasing share of oaks suggests a spatially more uneven intensity of the OLB infestation as the oak stands are further apart. This is confirmed also by the *in situ* records which on numerous occasions stated that "*the infestation is strong at the border of the forest compartment, but decreases as one goes deeper into the forest stand*" implying that forest compartments which are further away from roads are affected less or probably at a later time. These observations also speak in favour of the hypothesis that humans are a major vector responsible for the spread of the OLB.

Furthermore, the coarse resolution of the applied remote sensing data (MODIS) strongly hinders its applicability, since resampling of the *in situ* data (which is usually a point data) to the coarse grid of the remote sensing dataset (in our case 250 m pixel) introduces an additional source of errors.

Moreover, the extent of the damage associated with the OLB-related decrease in the photosynthetic capacity of the forest is not easily assessed with ground observations, in particular in the case of forests with different oak species and different admixture of other tree species. The observation of the damage in the visible range of the spectra (leaf discolouration) may not reflect the actual reduction in leaf photosynthetic capacity which could be larger or smaller than it visually appears. Unlike the *in situ* observations of the defoliation, which are relatively easy, the ground assessment inside the forest stand of the OLB damage to the leaves that are high above in the canopy is difficult. All this resulted that the *in situ* observations of the OLB pest occurrence, when translated to the MODIS pixel-level, were of limited accuracy with unknown uncertainty. Nevertheless, even such imperfect *in situ* data were of great value as they facilitated comparison with the detection based on remote sensing and modelling. In that light, the achieved agreement ranging from 73.9% (*RS*, C-flag 2 or 3, 2019) to 77.3% (both *MR* methods) in the case of Hungary and 61.1% (*MR*, C-flag 3, 2019) to 93.8% (*RS*, C-flag 2 or 3) in case of Croatia could justify the use of the presented methods for the OLB detection. These results are comparable with results from other studies, e.g. with Spruce et al. (2011) who reported 79.1 – 88.4% overall agreements for gypsy moth detection with different MODIS NDVI products.

Despite the mentioned issues of validation with the *in situ* data, the presented agreement between the independent *RS* and *MR* detection methods (Table 5) proves the presence of an agent causing a strong negative NDVI decrease in the region. The presented correlation between the residuals and the oaks share (Fig. 9) corroborates our hypothesis that the OLB is the main cause for the observed NDVI decrease.

The data measured by the Multispectral Instruments (MSI) on-board the European Sentinel-2A and 2B (Drusch et al., 2012) with its fine spatial (10–60 m) and temporal (10-day, or 5-day if combined) resolution could provide more detailed spatial detection and would suit better also to the validation with the *in situ* data. However, the MSI data were available only from the summer of 2015 (Sentinel-2A) and spring of 2017 (Sentinel 2B), therefore the length of the Sentinel data time-series

was not sufficient for our study. This also confirms the remarkable value of the long MODIS time-series.

4.5. Magnitude and the interannual variability of the OLB damage

Weather conditions affect the important life stages of the herbivore insects, affecting also the extent and intensity of the caused damage (Klapwijk et al., 2013). Generally, the higher temperatures and the reduced precipitation could be more favourable for the new invasive insect species (Koricheva et al., 1998, Rouault et al., 2006; Vanhanen et al., 2007). In the case of the OLB, the warmer and drier summers could increase the potential for complete development of more (even three) generations during the same growing season, but the weather could also have a possible positive effect on the quality of the food (sap) from the plants (Koricheva et al., 1998). In rainy years (in addition to the cooler weather affecting the insect physiology), the chance for the OLB of being washed away from the leaf significantly increases and the higher moisture contributes also to the susceptibility to fungi infections (Dreistadt and Perry, 2014). As a result, the insect damage in drought years can be *a priori* higher (Csóka et al., 1996, 1997; Jactel et al., 2012).

The OLB damage assessed within this study reflects the damage symptoms only in the investigated period 30–32 (21st Aug – 12th Sep), however, the decrease persists and increases until the senescence (Fig. 6). For *Pure pedunculate oak* stands in Croatia in the last 5 years of the study period the relative NDVI decrease due to the OLB was between 8.1% – 14.5% (Table 5). This is a considerable reduction, which must have an impact on the carbon cycle. For the complete assessment of the damage it will be necessary to consider the whole growing season, but also to use other tools such as MODIS GPP. Further research on the magnitude of the OLB damage, in relation to the meteorological conditions, is pending.

The most reliable way to assess the impact of the OLB on forest productivity would be from tree cores or long enough CO_2 flux measurements with eddy covariance (EC), similarly to Olsson et al., 2017. However, there is no such facility within our study area, but an EC flux tower exists and is running since 2008 approx. 50 km to the west of the study area, in the Jastrebarsko oak forest (Anić et al., 2018). Considering that in 2020 the OLB was already recorded in the Jastrebarsko forest as well (personal observation), the first EC estimates of the decrease in forest GPP due to OLB could be available soon.

4.6. Map of the detected spread

Mapping the spread of any pest by aerial or space-borne remote sensing techniques has great importance since it enables monitoring of possible pest infestation over large areas almost instantaneously and in a uniform way. In our case, the applied 95% threshold for forest share hindered the mapping of OLB infestation for the less forested areas where the OLB might be present, but with the benefit of increased reliability of the detection. The coarse-resolution MODIS data is not appropriate for a very detailed mapping of the infestation, in particular in the case of heterogeneous and patchy forests, as it was concluded by Olsson et al. (2016a, 2016b), too. But in the case of regional-scale infestations, our results confirm the usefulness of MODIS data. Nevertheless, the *in situ* ground observations, particularly if conducted according to a standardized protocol, should still be considered a gold standard in the mapping of the actual spread. As we have witnessed in the case of the Spačva forest (Fig. 11), the OLB likely arrived a few years before the first detection with MODIS, but at a low population density, the OLB damage was not sufficiently large to be detectable.

Based on both the *RS* and *MR* methods the detected OLB spread (with C-flag 3) from the initial place of the origin shows signs of acceleration (Fig. 12). Although the spread might be promoted by the increasing temperatures (Lange et al., 2006), it is probably affected mostly by the geographical distribution of oak forests and facilitated primarily by humans and our transport system (Rullan-Silva et al., 2013). The indication for this is the place of the origin of the OLB infestation in our study area (in the vicinity of the gas and resting station near a border crossing on the highway), but also the observed speed of its spread. It took 3 to 4 years for the infestation to spread within ~20 km radius to the entire Spačva forest, but in the next three years, the mean radius of infestation was already >100 km (Fig. 12). In other words, the natural speed of the OLB infestation spread in a closed forest with very low traffic intensity would likely be up to 5 km y^{-1}. However, the heavy traffic in combination with the huge source of the OLB (such as the Spačva forest was from 2015) was likely the main reason for the strong acceleration of the OLB spread from 2016 onwards.

5. Conclusions

The OLB causes a significant NDVI decrease in the late summer which can be used for detection of the infestation using MODIS. The optimal time for the detection in the study area corresponds to the 21st of August – 12th of September. Due to the coarse resolution of the MODIS data, the focus should be on the pixels with high forest share from large continuous forest areas.

The two novel methods for the detection of the OLB infestation presented in this study show a good 61.1% to very good 93.8% agreement with the *in situ* data, in particular in forests with high oak share. The presented *RS* method for the identification of the OLB infestation is based solely on the remotely sensed MODIS NDVI – it is simple, it can be used for near real-time detection, and it has good agreement with the more elaborated model residual (*MR*) method. The *MR* method with simple linear models of the NDVI in the selected period, made using a robust *Lasso* technique, takes into account the effects of the meteorology and soil water content and supports the more accurate assessment of the OLB damage manifested as pronounced NDVI decrease in the late summer.

The damage attributed to the OLB is significant (NDVI decrease down to -14.5% in pure pedunculate oak forests) and persistent after the infestation has started. Further research focusing on the effects of the OLB on the carbon cycle (e.g. with eddy covariance measurements or MODIS GPP) is highly needed as the infestation continues to progress to Western Europe.

Retracing the origin of the infestation to a location near to a gas and resting station on the Pan-European Corridor X from Southeastern to Western Europe corroborates the assumption that the arrival of the OLB in the study area and its further spread was primarily facilitated by the human transport system. The speed of the spread has been greatly augmented after the majority of the Spačva oak forest (>40 kha) became infested with the OLB, thus becoming a massive source of the OLB.

Author contribution

A.K. and H.M. conceptualized the study, analysed the results and wrote the first draft; A.K. processed the remote sensing, meteorological and Hungarian land cover data; H.M. processed the Croatian forest dataset, constructed models and performed statistical analysis; N.M. provided *in situ* data for Hungary; All authors improved the manuscript and approved the final version.

Declaration of Competing Interest

The authors declare that they have no known competing financial interests or personal relationships that could have appeared to influence the work reported in this paper.

Acknowledgements

The research has been supported by the Hungarian Scientific Research Fund (OTKA FK-128709), by the Croatian Science Foundation projects EFFEctivity (HRZZ UIP-2013-11-2492) and MODFLUX (HRZZ

IP-2019-04-6325), and by the János Bolyai Research Scholarship of the Hungarian Academy of Sciences (grant no. BO/00254/20/10). We thank NASA, for producing and distributing the MOD09 products. We are grateful to the Lechner Institute in Hungary for producing and freely disseminating the *National Ecosystem Base Map* land cover dataset of Hungary, created within the NÖSZTÉP Project. Special thanks to dr. Róbert Lehoczky for his kind help with the NÖSZTÉP dataset. The *in situ* data for Croatia were provided by the IPP database financed by the Croatian Ministry of Agriculture. We are grateful to Croatian Forest Ltd. company for granting H.M. access to the Croatian forests database. Last but not least, we are grateful to dr. Zoltán Barcza for his most valuable advice to the research. The authors would like to thank the two anonymous reviewers for their constructive comments that helped to improve the quality of the manuscript.

Supplementary materials

Supplementary material associated with this article can be found, in the online version, at doi:10.1016/j.agrformet.2021.108436.

References

Ahrens, A., Hansen, C.B., Schaffer, M.E., 2020. lassopack: model selection and prediction with regularized regression in Stata. Stata J. 20 (1), 176–235. https://doi.org/10.1177/1536867X20909697.

Anderegg, W.R.L., Hicke, J.A., Fisher, R.A., Allen, C.D., Aukema, J., Bentz, B., Hood, S., Lichstein, J.W., Macalady, A.K., McDowell, N., Pan, Y.D., Raffa, K., Sala, A., Shaw, J. D., Stephenson, N.L., Tague, C., Zeppel, M., 2015. Tree mortality from drought, insects, and their interactions in a changing climate. New Phytol. 208 (3), 674–683. https://doi.org/10.1111/nph.13477.

Anić, M., Ostrogović Sever, M.Z., Alberti, G., Balenović, I., Paladinić, E., Peressotti, A., Tijan, G., Večenaj, Ž., Vuletić, D., Marjanović, H., 2018. Eddy covariance vs. biometric based estimates of net primary productivity of pedunculate oak (*Quercus robur* L.) forest in Croatia during ten years. Forests 9, 764. https://doi.org/10.3390/f9120764.

Barber, N.A., 2010. Light environment and leaf characteristics affect distribution of *Corythucha arcuata* (Hemiptera: Tingidae). Environ. Entomol. 39, 492–497. https://doi.org/10.1603/EN09065.

Barka, I., Lukeš, P., Bucha, T., Hlásny, T., Strejček, R., Mlčoušek, M., Křístek, Š., 2018. Remote sensing-based forest health monitoring systems – case studies from Czechia and Slovakia. Cent. Eur. For. J. 64 (3–4), 259–275. https://doi.org/10.1515/forj-2017-0051.

Barić, L., Županić, M., Pernek, M., Diminić, D., 2012. First records of Chalara fraxinea in Croatia - a new agent of ash dieback (*Fraxinus* spp.). Šumar. List 136 (9–10), 461–469.

Balsamo, G., Beljaars, A., Scipal, K., Viterbo, P., van den Hurk, B., Hirschi, M., Betts, A.K., 2009. A revised hydrology for the ECMWF model: verification from field site to terrestrial water storage and impact in the integrated forecast system. J. Hydrometeorol. 10, 623–643. https://doi.org/10.1175/2008JHM1068.1.

de Beurs, K.M., Townsend, P.A., 2008. Estimating the effect of gypsy moth defoliation using MODIS. Rem. Sens. Environ. 112 (10), 3983–3990. https://doi.org/10.1016/j.rse.2008.07.008.

Bernardinelli, I., 2000. Distribution of the oak lace bug *Corythucha arcuata* (Say) in northern Italy (Heteroptera Tingidae). Redia 83, 157–162.

Bernardinelli, I., Zandigiacomo, P., 2000. Prima segnalazione di *Corythucha arcuata* (Say) (Heteroptera, Tingidae) in Europe. Inf. Fitopatol. 12, 47–49.

Bright, B.C., Hicke, J.A., Meddens, A.J.H., 2013. Effects of bark beetle-caused tree mortality on biogeochemical and biogeophysical MODIS products. J. Geophys. Res. Biogeosci. 118, 974–982. https://doi.org/10.1002/jgrg.20078.

Chávez, R.O., Rocco, R., Gutiérrez, Á.G., Dörner, M., Estay, S.A., 2019. A self-calibrated non-parametric time series analysis approach for assessing insect defoliation of broad-leaved deciduous nothofagus pumilio forests. Remote Sens. 11 (2), 204. https://doi.org/10.3390/rs11020204.

Chen, J., Jönsson, P., Tamura, M., Gu, Z., Matsushita, B., Eklundh, L., 2004. A simple method for reconstructing a high-quality NDVI time-series data set based on the Savitzky–Golay filter. Rem. Sens. Environ. 91 (3–4), 332–344. https://doi.org/10.1016/j.rse.2004.03.014.

Editors: Chen, G., Meentemeyer, R.K., 2016. Remote sensing of forest damage by diseases and insects. In: Weng, Qihao (Ed.), Remote Sensing for Sustainability. CRC Press, pp. 145–162. https://doi.org/10.1201/9781315371931-9. doi:10.1201/9781315371931.

COM, 2020a. Proposal for a Regulation of The European Parliament and of The Council Establishing the Framework for Achieving Climate Neutrality and Amending Regulation (EU) 2018/1999 (European Climate Law). European Commission, COM, Brussels (2020)80 final. https://eur-lex.europa.eu/legal-content/EN/TXT/?uri=CELEX:52020PC0080.

COM, 2020b. Inception Impact Assessment. European Commission, Brussels. Ref. Ares (2020)6081753 - 29/10/2020. https://ec.europa.eu/info/law/better-regulation/have-your-say/initiatives/12657-Land-use-land-use-change-and-forestry-review-of-EU-rules.

Connell, W.A., Beacher, J.H., 1947. Life history and control of the oak lace bug. Bulletin of the University of Delaware Agricultural Experiment Station, p. pp. 28. No. 265.

CCCS, 2019. Copernicus Climate Change Service: ERA5-Land hourly data from 2001 to present [Data set]. ECMWF. doi:10.24381/CDS.E2161BAC, URL: https://cds.climate.copernicus.eu/cdsapp#!/dataset/reanalysis-era5-land?tab=overview (Accessed on 16th of March, 2020).

Csepelényi, M., Hirka, A., Mikó, Á., Szalai, Á., Csóka, Gy., 2017a. Overwintering success of the oak lace bug (*Corythucha arcuata*) in 2016/2017 at South-Eastern Hungary. Növényvédelem 78 (53), 285–288, 7.

Csepelényi, M., Hirka, A., Szénási, Á., Mikó, Á., Szőcs, L., Csóka, Gy., 2017b. Rapid area expansion and mass occurrences of the invasive oak lace bug [*Corythucha arcuate* (Say 1832)] in Hungary (In Hungarian: Az inváziós tölgycsipkéspoloska [*Corythucha Arcuata* (Say, 1832)] gyors terjeszkedése és tömeges fellépése Magyarországon). Erdészettudományi Közlemények 7, 2.doi:10.17164/EK.2017.009127–134.

Csóka, Gy., 1996. Aszályos évek - fokozódó rovarkárok erdeinkben (years of drought – increasing damage by forest insects). Növényvédelem 32, 545–551.

Csóka, Gy., 1997. Increased insect damage in Hungarian forests under drought impact. Biologia 52, 1–4.

Csóka, Gy., Hirka, A., Somlyai, M., 2013. A tölgy csipkéspoloska (*Corythucha arcuata*, Say 1832 – hemiptera, tingidae) első észlelése Magyarországon. Növényvédelem 49 (7), 293–296.

Csóka, Gy., Pödör, Z., Nagy, G., Hirka, A., 2015. Canopy recovery of pedunculate oak, Turkey oak and beech trees after severe defoliation by gypsy moth (*Lymantria dispar*): case study from Western Hungary. Cent. Eur. For. J. 61 (3), 143–148. https://doi.org/10.1515/forj-2015-0022.

Csóka, Gy., Hirka, A., Mutun, S., Glavendekić, M., Mikó, Á., Szőcs, L., Paulin, M., Eötvös, C.B., Gáspár, C., Csepelényi, M., Szénási, Á., Franjević, M., Gninenko, Y., Dautbašić, M., Muzejinović, O., Zúbrik, M., Netoiu, C., Buzatu, A., Bălăcenoiu, F., Jurc, M., Jurc, D., Bernardinelli, I., Streito, J.-C., Avtzis, D., Hrašovec, B., 2020. Spread and potential host range of the invasive oak lace bug [*Corythucha arcuata* (Say, 1832) – Heteroptera: Tingidae] in Eurasia. Agric. For. Entomol. 22, 61–74. https://doi.org/10.1111/afe.12362.

Dietze, J., Matthes, H., 2014. A general ecophysiological framework for modelling the impact of pests and pathogens on forest ecosystems. Ecol. Lett. 17, 1418–1426. https://doi.org/10.1111/ele.12345.

Dobor, L., Barcza, Z., Hlásny, T., Havasi, Á., Horváth, F., Ittzés, P., Bartholy, J., 2014. Bridging the gap between climate models and impact studies: the FORESEE database. Geosci. Data J. 2, 1–11. https://doi.org/10.1002/gdj3.22.

Dobreva, M., Simov, N., Georgiev, G., Mirchev, P., Georgieva, M., 2013. First record of *Corythucha arcuata* (Say) (Heteroptera: Tingidae) on the Balkan Peninsula. Acta Zool. Bulg. 65 (3), 409–412.

Dreistadt, S.H., Perry, E.J., 2014. Lace bugs: integrated pest management for home gardeners and landscape professionals. Pest Notes, University of California Agricultural and Natural Resources, Bulletin, pp. 1–4.

Drusch, M., Bello, U.D., Carlier, S., Colin, O., Fernandez, V., Gascon, F., Hoersch, B., Isola, C., Laberinti, P., Martimort, P., Meygret, A., Spoto, F., Sy, O., Marchese, F., Bargellini, P., 2012. Sentinel-2: ESA's optical high-resolution mission for GMES operational services. Rem. Sens. Environ. 120, 25–36. https://doi.org/10.1016/j.rse.2011.11.026.

Eklundh, L., Johansson, T., Solberg, S., 2009. Mapping insect defoliation in Scots pine with MODIS time-series data. Rem. Sens. Environ. 113 (7), 1566–1573. https://doi.org/10.1016/j.rse.2009.03.008.

Franjević, M., Drvodelić, D., Kolar, A., Gradečki-Poštenjak, M., Hrašovec, B., 2018. Impact of oak lace bug *Corythucha arcuata* (Heteroptera: Tingidae) on pedunculate oak (*Quercus robur*) seed quality. . In I. Radojčić Redovniković, T. Jakovljević, V. Petravić Tominac, et al. (Eds.), Natural Resources Green Technology & Sustainable Development -GREEN/3. pp. 161-165. https://urn.nsk.hr/urn:nbn:hr:108:973656.

Fraser, R.H., Abuelgasim, A., Latifovic, R., 2005. A method for detecting large-scale forest cover change using coarse spatial resolution imagery. Rem. Sens. Environ. 95 (4), 414–427. https://doi.org/10.1016/j.rse.2004.12.014.

Griffiths, P., Kuemmerle, T., Baumann, M., Radeloff, V.C., Abrudan, I.V., Lieskovsky, J., Munteanu, C., Ostapowicz, K., Hostert, P., 2014. Forest disturbances, forest recovery, and changes in forest types across the Carpathian ecoregion from 1985 to 2010 based on Landsat image composites. Rem. Sens. Environ. 151, 72–88. https://doi.org/10.1016/j.rse.2013.04.022.

Hargrove, W.W., Spruce, J.P., Gasser, G.E., Hoffman, F.M., 2009. Toward a national early warning system for forest disturbances using remotely sensed canopy phenology. Photogram. Eng. Rem. S. 75, 1150–1156.

Hayes, D.J., Cohen, W.B., Sader, S.A., Irwin, D.E., 2008. Estimating proportional change in forest cover as a continuous variable from multi-year MODIS data. Rem. Sens. Environ. 112 (3), 735–749. https://doi.org/10.1016/j.rse.2007.06.003.

Hicke, J.A., Allen, C.D., Desai, A.R., Dietze, M.C., Hall, R.J., Hogg, E.H., Kashian, D.M., Moore, D., Raffa, K.F., Sturrock, R.N., Vogelmann, J., 2012. Effects of biotic disturbances on forest carbon cycling in the United States and Canada. Glob. Change Biol. 18 (1), 7–34. https://doi.org/10.1111/j.1365-2486.2011.02543.x.

Hlásny, T., Turčáni, M., 2008. Insect pests as climate change driven disturbances in forest Ecosystems. In: Střelcová K. et al. (eds) Bioclimatology and Natural Hazards. Springer, Dordrecht. doi:10.1007/978-1-4020-8876-6_15.

Hrašovec, B., Posaric, D., Lukic, I., Pernek, M., 2013. First record of oak lace bug (*Corythucha arcuata*) in Croatia (Prvi nalaz hrastove mrežaste stjenice (*Corythucha arcuata*) u Hrvatskoj). Prethodno priopcenje – Preliminary communication. Šumar. List 9–10, 499–503.

Huete, A., Liu, H.Q., van Leeuwen, J.D., 1997. The use of vegetation indices in forested regions: issues of linearity and saturation. IEE Trans. Geosci. Remote Sens. In:

Proceedings of IGARSS '97 — International Geosciences and Remote Sensing Seminar. ESA Publications, Noordwijk, The Netherlands, pp. 1966–1968.
Huete, A., Didan, K., Miura, T., Rodriguez, E.P, Gao, X., Ferreira, L.G., 2002. Overview of the radiometric and biophysical performance of the MODIS vegetation indices. Rem. Sens. Environ. 83 (1–2), 195–213. https://doi.org/10.1016/S0034-4257(02)00096-2.
Imanyfar, S., Hasanlou, M., Zadeh, V.M., 2019. Mapping oak decline through long-term analysis of time series of satellite images in the forests of Malekshahi, Iran. Int. J. Remote Sens. 40 (23), 8705–8726. https://doi.org/10.1080/01431161.2019.1620375.
Jactel, H., Petit, J., Desprez-Loustau, M.-L., Delzon, S., Piou, D., Battisti, A., Koricheva, J., 2012. Drought effects on damage by forest insects and pathogens: a meta-analysis. Glob. Change Biol. 18, 267–276. https://doi.org/10.1111/j.1365-2486.2011.02512.x.
Jin, S., Sader, S.A., 2005. MODIS time-series imagery for forest disturbance detection and quantification of patch size effects. Rem. Sens. Environ. 99 (4), 462–470. https://doi.org/10.1016/j.rse.2005.09.017.
Justice, C.O., Vermote, E., Townshend, J.R.G., Defries, R., Roy, D.P., Hall, D.K., Salomonson, V.V., Privette, J.L., Riggs, G., Strahler, A., et al., 1998. The moderate resolution imaging spectroradiometer (MODIS): land remote sensing for global change research. Trans. Geosci. Remote Sens. 36, 1228–1249. https://doi.org/10.1109/36.701075.
Kern, A., Marjanović, H., Barcza, Z., 2016. Evaluation of the quality of NDVI3g dataset against Collection 6 MODIS NDVI in Central-Europe between 2000 and 2013. Remote Sens. 8, 955. https://doi.org/10.3390/rs8110955.
Kern, A., Marjanović, H., Dobor, L., Anic, M., Hlásny, T., Barcza, Z., 2017. Identification of years with extreme vegetation state in Central Europe based on remote sensing and meteorological data. South-east European forestry (SEEFOR) 8, 1–20. https://doi.org/10.15177/seefor.17-05.
Kern, A., Marjanović, H., Barcza, Z., 2020. Spring vegetation green-up dynamics in Central Europe based on 20-year long MODIS NDVI data. Agric. For. Meteorol. 287, 107969 https://doi.org/10.1016/j.agrformet.2020.107969.
Klapwijk, M.J., Csóka, Gy., Hirka, A., Björkman, C., 2013. Forest insects and climate change: long-term trends in herbivore damage. Ecol. Evol. 3 (12), 4183–4196. https://doi.org/10.1002/ece3.717.
Klepac, D., Fabijanić, G., 1996. Management of pedunculate oak forests. In: Klepac, D., Dundović, J., Gračan, J. (Eds.), Pedunculate Oak in Croatia, 1st ed. Croatian Academy of Arts and Sciences, Centre for Scientific Work, Vinkovci and Croatian Forests Ltd., Zagreb, Croatia, pp. 452–457. , ISBN 953-154-079-9.
Koricheva, J., Larsson, S., Haukioja, E., 1998. Insect performance on experimentally stressed woody plants: a meta-analysis. Annu. Rev. Entomol. 43, 195–216. https://doi.org/10.1146/annurev.ento.43.1.195.
Kovač, M., Gorczak, M., Wrzosek, M., Tkaczuk, C., Pernek, M., 2020. Identification of entomopathogenic fungi as naturally occurring enemies of the invasive oak lace bug, *Corythucha arcuata* (Say) (Hemiptera: Tingidae). Insects 11, 679. https://doi.org/10.3390/insects11100679.
Lange, H., Okland, B., Krokene, P., 2006. Thresholds in the life cycle of the spruce bark beetle under climate change. Int. J. Complex Syst. 1648, 1–10.
LP DAAC (Land Processes Distributed Active Archive Center), 2020 MOD09A1, Collection 6. NASA EOSDIS Land Processes DAAC, USGS Earth Resources Observation and Science (EROS) Center, Sioux Falls, South Dakota. URL: https://lpdaac.usgs.gov (Accessed on 14th of January, 2020).
Lunetta, R.S., Knight, J.F., Ediriwickrema, J., Lyon, J.G., Worthy, L.D., 2006. Land-cover change detection using multi-temporal MODIS NDVI data. Rem. Sens. Environ. 105 (2), 142–154. https://doi.org/10.1016/j.rse.2006.06.018.
Matošević, D., 2012. The Reporting and Forecasting in Forestry for the Year 2011/2012 (Izvještajno prognozni poslovi u šumarstvu za 2011/12. godinu, In Croatian), 2012. Croatian Forest Research Institute, Jastrebarsko, p. 82. URL. https://stetnici.sumins.hr/Blog/godisnje_izvjesce_ipp-a_u_sumarstvu_za_2011_godinu. Accessed on 16th of November, 2020.
Matošević, D., 2020. The Reporting and Forecasting in Forestry for the Year 2019 (Izvještajno prognozni poslovi u šumarstvu za 2019/2020. godinu, In Croatian). Croatian Forest Research Institute, Jastrebarsko, p. 92. URL. https://stetnici.sumins.hr/Blog/godisnje_izvjesce_ipp-a_za_2019_godinu. Accessed on 16th of November, 2020.
McNemar, Q., 1947. Note on the sampling error of the difference between correlated proportions or percentages. Psychometrika 12, 153–157. https://doi.org/10.1007/BF02295996.
Meng, R., Dennison, P.E., Zhao, F., Shendryk, I., Rickert, A., Hanavan, R.P., Cook, B.D., Serbin, S.P., 2018. Mapping canopy defoliation by herbivorous insects at the individual tree level using bi-temporal airborne imaging spectroscopy and LiDAR measurements. Rem. Sens. Environ. 215, 170–183. https://doi.org/10.1016/j.rse.2018.06.008.
Mertelík, J., Liška, J., 2020. Faunistic records from the Czech Republic – Hemiptera: Heteroptera: Tingidae. Klapalekiana 56, 1–2. *In press*.
Misra, S., Osogba, O., Powers, M., 2020. Chapter 1 - unsupervised outlier detection techniques for well logs and geophysical data (editors). In: Misra, S., Li, H., He, J. (Eds.), Machine Learning for Subsurface Characterization. Gulf Professional Publishing, pp. 1–37.
Moreau, G., Achim, A., Pothier, D., 2020. An accumulation of climatic stress events has led to years of reduced growth for sugar maple in southern Quebec, Canada. Ecosphere 11 (7). https://doi.org/10.1002/ecs2.3183.
NFK, 2020. Hungarian National Forest Damage Registration System. Available at: http://www.nfk.gov.hu/Adatszolgaltatasi_kotelezettseg_az_Orszagos_Erdokar_Nyilvantartasi_Rendszerbe_news_326. Accessed on 1th of May.
Nikolić, N., Pilipović, A., Drekić, M., Kojić, D., Poljaković-Pajnik, L., Orlović, S., Arsenov, D., 2019. Physiological responses of Pedunculate oak (*Quercus robur* L.) to *Corythucha arcuata* (Say, 1832) attack. Arch. Biol. Sci. 71 (1), 167–176. https://doi.org/10.2298/ABS180927058N.
Olsson, P.-O., Kantola, T., Lyytikäinen-Saarenmaa, P., Jönsson, A.M., Eklundh, L., 2016a. Development of a method for monitoring of insect induced forest defoliation – limitation of MODIS data in Fennoscandian forest landscapes. Silva Fenn 50 (2), 1495. https://doi.org/10.14214/sf.1495.
Olsson, P.-O., Lindström, J., Eklundh, L., 2016b. Near real-time monitoring of insect induced defoliation in subalpine birch forests with MODIS derived NDVI. Rem. Sens. Environ. 181, 42–53. https://doi.org/10.1016/j.rse.2016.03.040.
Olsson, P.-O., Heliasz, M., Jin, H., Eklundh, L., 2017. Mapping the reduction in gross primary productivity in subarctic birch forests due to insect outbreaks. Biogeosciences 14, 1703–1719. https://doi.org/10.5194/bg-14-1703-2017.
Paulin, M., Hirka, A., Eötvös, Cs.B., Gáspár, Cs., Fürjes-Mikó, Á., Csóka, Gy., 2020. Known and predicted impacts of the invasive oak lace bug (*Corythucha arcuata*) in European oak ecosystems – a review. Folia Oecologica 47 (2). https://doi.org/10.2478/foecol-2020-0015.
Rouault, G., Candau, J-N., Lieutier, F., Nageleisen, L-M., Martin, J-C., Warzée, N., 2006. Effects of drought and heat on forest insect populations in relation to the 2003 drought in Western Europe. Ann. For. Sci. 63 (6), 613–624. https://doi.org/10.1051/forest:2006044.
Rubel, F., Kottek, M., 2010. Observed and projected climate shifts 1901–2100 depicted by world maps of the Köppen-Geiger climate classification. Meteorol. Z. 19, 135–141. https://doi.org/10.1127/0941-2948/2010/0430.
Rullan-Silva, C.D., Olthoff, A.E., Delgado de la Mata, J.A., Pajares-Alonso, J.A., 2013. Remote monitoring of forest insect defoliation - a review. For. Syst. 22, 377–391. https://doi.org/10.5424/fs/2013223-04417.
Sangüesa-Barreda, G., Camarero, J.J., García-Martín, A., Hernández, R., de la Riva, J., 2014. Remote-sensing and tree-ring based characterization of forest defoliation and growth loss due to the Mediterranean pine processionary moth. For. Ecol. Manag. 320, 171–181. https://doi.org/10.1016/j.foreco.2014.03.008.
Santos, J.A., Malheiro, A.C., Karremann, M.K., Pinto, J.G., 2011. Statistical modelling of grapevine yield in the Port Wine region under present and future climate conditions. Int. J. Biometeorol. 55, 119–131. https://doi.org/10.1007/s00484-010-0318-0.
Seidl, R., Schelhaas, M., Rammer, W., Verkerk, P.J., 2014. Increasing forest disturbances in Europe and their impact on carbon storage. Nat. Clim. Change 4, 806–810. https://doi.org/10.1038/NCLIMATE2318.
Shen, M., Piao, S., Cong, N., Zhang, G., Jassens, I.A., 2015. Precipitation impacts on vegetation spring phenology on the Tibetan Plateau. Glob. Chang. Biol. 21, 3647–3656. https://doi.org/10.1111/gcb.12961.
Simov, N., Grozeva, S., Langouro, M., Georgieva, M., Mirchev, P., Georgiev, G., 2018. Rapid expansion of the Oak lace bug *Corythucha arcuata* (Say, 1832) (Hemiptera: Tingidae) in Bulgaria. Historia Naturalis Bulgarica 2, 51–55.
Solberg, S., Næsset, E., Hanssen, K.H., Christiansen, E., 2006. Mapping defoliation during a severe insect attack on Scots pine using airborne laser scanning. Rem. Sens. Environ. 102, 364–376. https://doi.org/10.1016/j.rse.2006.03.001.
Somogyi, Z., Koltay, A., Molnár, T., Móricz, N., 2018. Forest Health Monitoring System in Hungary Based on MODIS products. IX. Theory Meets Practice in GIS. Debrecen, Hungary, pp. 325–330. ISBN 978 963-318-723-4.
Sotirovski, K., Srebrova, K., Nacheski, S., 2019. First records of the oak lace bug *corythucha arcuata* (Say, 1832) (Hemiptera: Tingidae) in North Macedonia. Acta Entomol. Sloven. 27 (2), 91–98.
Spruce, J.P., Sader, S., Ryan, R.E., Smoot, J., Kuper, P., Ross, K., Prados, R., Russell, J., Gasser, G., McKellip, R., Hargrove, W., 2011. Assessment of MODIS NDVI time series data products for detecting forest defoliation by gypsy moth outbreaks. Rem. Sens. Environ. 115 (2), 427–437. https://doi.org/10.1016/j.rse.2010.09.013.
Spruce, J.P., Hicke, J.A., Hargrove, W.W., Grulke, N.E., Meddens, A.J.H., 2019. Use of MODIS NDVI products to map tree mortality levels in forests affected by mountain pine beetle outbreaks. Forests 10, 811. https://doi.org/10.3390/f10090811.
Szabó, I., 2008. A magas kőris Chalara fraxinea okozta hajtás- és vesszőpusztulásának megjelenése Magyarországon. Növényvédelem 44 (9), 444–446.
Tanács, E., Belényesi, M., Lehoczki, R., Pataki, R., Petrik, O., Standovár, T., Pásztor, L., Laborczi, A., Szatmári, G., Molnár, Zs., Bede-Fazekas, Á., Kisné Fodor, L., Varga, I., Zsembery, Z., Maucha, G., 2019. A national, high-resolution ecosystem basemap: methodology, validation, and possible uses. Term. Közl. 25, 34–58. https://doi.org/10.17779/tvk-jnatconserv.2019.25.34.
Tan, B., Woodcock, C.E., Hu, J., Zhang, P., Ozdogan, M., Huang, D., Yang, W., Knyazikhin, Y., Myneni, R.B., 2006. The impact of gridding artifacts on the local spatial properties of MODIS data: Implications for validation, compositing, and band-to-band registration across resolutions. Rem. Sens. Environ. 105, 98–114. https://doi.org/10.1016/j.rse.2006.06.008.
Thornton, P.E., Hasenauer, H., White, M.A., 2000. Simultaneous estimation of daily solar radiation and humidity from observed temperature and precipitation: an application over complex terrain in Austria. Agric. For. Meteorol. 104, 255–271. https://doi.org/10.1016/S0168-1923(00)00170-2.
Tibshirani, R., 1996. Regression shrinkage and selection via the Lasso. J. R. Stat. Soc.. Ser. B (Methodol.) 58 (1), 267–288. Retrieved October 18, 2020, from. http://www.jstor.org/stable/2346178.

Tomescu, R., Olenici, N., Netoiu, C., Balacenoiu, F., Buzatu, A., 2018. Invasion of the oak lace bug *Corythucha arcuata* (Say.) in Romania: a first extended reporting. Ann. For. Res. 61 (2), 161–170. https://doi.org/10.15287/afr.2018.1187.

Townsend, P.A., Singh, A., Foster, J.R., Rehberg, N.J., Kingdon, C.C., Eshleman, K.N., Seagle, S.W., 2012. A general Landsat model to predict canopy defoliation in broadleaf deciduous forests. Rem. Sens. Environ. 119, 255–265. https://doi.org/10.1016/j.rse.2011.12.023.

Vanhanen, H., Veteli, T.O., Paivinen, S., Kellomaki, S., Niemela, P., 2007. Climate change and range shifts in two insect defoliators: gypsy moth and nun moth - a model study. Silva Fennica 41 (4), 621–638. https://doi.org/10.14214/sf.469.

Verbesselt, J., Robinson, A., Stone, C., Culvenor, D., 2009. Forecasting tree mortality using change metrics derived from MODIS satellite data. For. Ecol. Manag. 258 (7), 1166–1173. https://doi.org/10.1016/j.foreco.2009.06.011.

Vermote, E., 2015. MOD09A1 MODIS/Terra Surface Reflectance 8-Day L3 Global 500m SIN Grid V006 [Data set]. NASA EOSDIS Land Processes DAAC. https://doi.org/10.5067/MODIS/MOD09A1.006 (Accessed on 23rd of May, 2018).

Viovy, N., Arino, O., Belward, A.S., 1992. The Best Index Slope Extraction (BISE): A method for reducing noise in NDVI time-series. Int. J. Remote Sens. 13 (8), 1585–1590. https://doi.org/10.1080/01431169208904212.

Wang, L., Tian, F., Wang, Y., Wu, Z., Schurgers, G., Fensholt, R., 2018. Acceleration of global vegetation greenup from combined effects of climate change and human land management. Glob. Chang. Biol. 24, 5484–5499. https://doi.org/10.1111/gcb.14369.

Wolf, A., Kozlov, M.V., Callaghan, T.V., 2008. Impact of non-outbreak insect damage on vegetation in northern Europe will be greater than expected during a changing climate. Clim. Change 87 (1–2), 91–106. https://doi.org/10.1007/s10584-007-9340-6.

Wolfe, R.E., Nishihama, M., Fleig, A.J., Kuyper, J.A., Roy, D.P., Storey, J.C., Patt, F.S., 2002. Achieving sub-pixel geolocation accuracy in support of MODIS land science. Rem. Sens. Environ. 83, 31–49. https://doi.org/10.1016/S0034-4257(02)00085-8.

Zeller, R.A., Levine, Z.H., 1974. The effects of violating the normality assumption underlying R. Sociol. Methods Res. 2 (4), 511–519. https://doi.org/10.1177/004912417400200406.